Retinal ganglion cell vulnerability to pathogenic tau in Alzheimer's disease

Miyah R. Davis[1], Edward Robinson[1], Yosef Koronyo[1], Elena Salobrar-Garcia[2], Altan Rentsendorj[1], Bhakta P. Gaire[1], Nazanin Mirzaei[1], Rakez Kayed[3,4], Alfredo A. Sadun[5,6], Alexander V. Ljubimov[1,7,8], Lon S. Schneider[9], Debra Hawes[9], Keith L. Black[1], Dieu-Trang Fuchs[1], Maya Koronyo-Hamaoui[1,8,10@]

[1]Department of Neurosurgery, Maxine Dunitz Neurosurgical Research Institute, Cedars-Sinai Medical Center, Los Angeles, CA, USA

[2]Institute of Ophthalmologic Research Ramón Castroviejo, Complutense University of Madrid, 28040 Madrid, Spain. Department of Immunology, Ophthalmology and ENT, Faculty of Optics and Optometry, Complutense University of Madrid, 28040 Madrid, Spain. Health Research Institute, Clinico San Carlos Hospital (IdISSC), 28040 Madrid, Spain.

[3]Mitchell Center for Neurodegenerative Diseases, University of Texas Medical Branch at Galveston, TX, USA

[4]Departments of Neurology, Neuroscience, and Cell Biology, University of Texas Medical Branch, Galveston, TX, USA

[5]Department of Ophthalmology, David Geffen School of Medicine at University of California Los Angeles, Los Angeles, CA, USA.

[6]Doheny Eye Institute, Los Angeles, CA, USA.

[7]Eye Program, Board of Governors Regenerative Medicine Institute, Cedars-Sinai Medical Center, Los Angeles, CA, USA

[8]Department of Biomedical Sciences, Division of Applied Cell Biology and Physiology, Cedars-Sinai Medical Center, Los Angeles, CA, USA

[9]Alzheimer's Disease Research Center, Keck School of Medicine, University of Southern California, Los Angeles, California, USA

[10]Department of Neurology, Cedars-Sinai Medical Center, Los Angeles, CA, USA

[@] Corresponding author: Maya Koronyo-Hamaoui, PhD, Cedars-Sinai Medical Center, 127 S. San Vicente Blvd., A6212, Los Angeles, CA, USA 90048. Tel: (310)-423-7473, E-mail: maya.koronyo@csmc.edu

Abstract

Accumulation of pathological tau isoforms, especially hyperphosphorylated tau at serine 396 (pS396-tau) and tau oligomers, has been demonstrated in the retinas of patients with mild cognitive impairment (MCI) and Alzheimer's disease (AD). Previous studies have noted a decrease in retinal ganglion cells (RGCs) in AD patients, but the presence and impact of pathological tau isoforms in RGCs and RGC integrity, particularly in early AD stages, have not been explored. To investigate this, we examined retinal superior temporal cross-sections from 25 patients with MCI (due to AD) or AD dementia and 16 cognitively normal (CN) controls, matched for age and gender. We utilized the RGC marker ribonucleic acid binding protein with multiple splicing (RBPMS) and Nissl staining to assess neuronal density in the ganglion cell layer (GCL). Our study found that hypertrophic RGCs containing pS396-tau and T22-positive tau oligomers were more frequently observed in MCI and AD patients compared to CN subjects. Quantitative analyses indicated a decline in RGC integrity, with 46-55% and 55-56% reductions of $RBPMS^+$ RGCs ($P<0.01$) and $Nissl^+$ GCL neurons ($P<0.01$-0.001), respectively, in MCI and AD patients. This decrease in RGC count was accompanied by increases in necroptotic-like morphology and the cleaved caspase-3 apoptotic marker in RGCs of AD patients. Furthermore, there was a 2.1 to 3.1-fold increase ($P<0.05$-0.0001) in pS396-tau-laden RGCs in MCI and AD patients, with a greater abundance observed in individuals with higher Braak stages (V-VI), more severe clinical dementia ratings (CDR=3), and lower mini-mental state examination (MMSE) scores. Strong correlations were noted between the decline in RGCs and the total amount of retinal pS396-tau and pS396-tau^+ RGCs, with pS396-tau^+ RGC counts correlating significantly with brain neurofibrillary tangle scores ($r= 0.71$, $P= 0.0001$), Braak stage ($r= 0.65$, $P= 0.0009$), and MMSE scores ($r= -0.76$, $P= 0.0004$). These findings suggest that retinal tauopathy, characterized by pS396-tau and oligomeric tau in hypertrophic RGCs, is associated with and may contribute to RGC degeneration in AD. Future research should validate these findings in larger cohorts and explore noninvasive retinal imaging techniques that target tau pathology in RGCs to improve AD detection and monitor disease progression.

Keywords: eye, tauopathy, amyloid beta, ganglion cell layer, retinal ganglion cells

Introduction

Alzheimer's disease (AD), the most prevalent and progressive form of senile dementia, affects an estimated 6.9 million Americans aged 65 and older [1]. It is characterized by the accumulation of amyloid beta-protein (Aβ) deposits and abnormal tau protein aggregates in the brain [18, 50]. During AD progression, microtubule-associated tau proteins undergo hyperphosphorylation (p-tau) and form toxic oligomers that spread between neurons, accelerating disease progression [14, 41, 42, 54, 58, 64]. These tau species eventually aggregate into neurofibrillary tangles (NFTs) [79], disrupting cellular functions and axonal transport, which leads to synaptic dysfunction and neuronal death [83, 95, 105, 116]. The presence of abnormal tau strongly correlates with the progression of neurodegeneration and cognitive deficits in AD [20, 35, 41, 51, 65]. AD neuropathology develops many years before neurobehavioral and cognitive disturbances become salient [51, 110, 111, 124], therefore early identification of AD pathological hallmarks in the central nervous system (CNS) is crucial for early intervention and disease management.

The retina, a posterior neurosensory eye tissue, is an extension of the brain and shares many structural and functional features with the brain. New studies have revealed the genetic basis for eye-brain connections, suggesting bidirectional genetic causal links between retinal structures and neurological disorders, including AD [33, 93, 127]. Growing evidence indicates the presence of AD-related pathological features in the retinas of patients with mild cognitive impairment (MCI due to AD) and/or AD dementia, including various abnormal Aβ and tau species, vascular damage, micro- and macro-gliosis, and neurodegeneration [2, 4, 6, 7, 16, 17, 22, 27, 29-31, 37, 40, 43, 46, 48, 60-62, 67, 70, 71, 81, 85, 86, 94, 103, 104, 106-108, 113, 122, 123]. Regarding tauopathy, a wide range of abnormal tau isoforms have been identified in the retinas of AD patients, including pretangles and mature tangle forms: 3- and 4-repeat tau, p-tau and citrullinated tau forms,

oligomeric tau, paired helical filaments (PHF) of tau, as well as paperclip folding of tau and NFT-like structures [27, 29, 40, 45, 46, 60, 86, 108, 122]. We recently found that the retinas of patients with MCI (due to AD) and/or AD dementia exhibit significant increases in pathogenic p-tau at specific epitopes, including S202/T205, S214, S396, S404, and T231, as well as citrullinated R209-tau and tau oligomers (T22-positive), alongside PHF^{+} and $MC\text{-}1^{+}$ pretangle and mature tau tangles. Epitopes S199 and T212/S214 did not show such changes [108]. Moreover, oligomeric tau and pS396-tau, commonly elevated in AD brains [96, 120], were consistently increased in AD retinas and strongly associated with more severe brain pathology, advanced disease stages, and cognitive decline [108]. However, the impact of AD-related tauopathy on specific retinal cell types in patients has not yet been described.

Retinal ganglion cells (RGCs) are neurons located in the retinal ganglion cell layer (GCL; as seen in optical coherence tomography – OCT imaging) and existing in various subtypes such as midget, parasol, bistratified, and melanopsin-containing intrinsically photosensitive RGCs (mRGCs). These cells serve diverse functions, including high spatial frequency resolution, color differentiation, low spatial frequency contrast, and photoentrainment of the hypothalamus, which governs circadian rhythms [102, 121]. Dendritic protrusions from the RGC soma receive synaptic input from the axons of bipolar and amacrine cells in the inner plexiform layer (IPL). The RGCs project their axons to form the nerve fiber layer (NFL), which collects at the optic discs and continues as the optic nerve. This pathway ultimately transmits all visual information to the brain [55]. Notably, the RGCs, located in the inner retinal surface, are uniquely positioned as neurons in the CNS that can be noninvasively imaged and quantitatively assessed in vivo with high resolution using the advanced adaptive optics (AO)-OCT technology, as demonstrated in recent studies [44,

76]. This advanced imaging capability enables detailed examination of RGC pathology and may facilitate future AD diagnosis and monitoring.

In the context of AD, pioneering studies have demonstrated the loss of RGCs in patients [15, 16, 48]. Other reports have shown visual dysfunctions such as impaired contrast sensitivity, abnormal color discrimination, and diminished visual fields, which can be attributed to RGC degeneration [37, 53, 97, 100, 118]. Subsequent investigations into the AD retina found NFL thinning, reduced density of melanopsin-containing RGCs, GCL cell loss, and elevated apoptotic markers, along with intraneuronal Aβ oligomers and other Aβ species within RGCs in these patients [4-6, 23, 25, 37, 56, 60, 61, 66, 67, 70, 74]. A recent report in several transgenic murine models of AD showed RGC susceptibility, manifested as RGC dendritic field reduction, occurring in parallel with hippocampal dendritic spine loss [13]. An additional study detected an increased total tau burden in RGCs in an AD-murine model [24]. However, the vulnerability of RGCs to pathogenic tau accumulation in AD patients, particularly in the earliest stages of functional impairment (MCI due to AD), and the potential relationships with disease status, have not yet been studied.

In the current study, we addressed these gaps by first investigating the density, size, and distribution of RGCs in the superior temporal postmortem retinas of patients with MCI (due to AD) and AD dementia, compared with cognitively normal (CN) individuals. We then explored whether AD-specific pathological tau forms, pS396-tau and oligomeric tau, are present specifically in RGCs, and quantified pS396-tau-containing RGCs in this cohort. The interplay between pS396-tau-containing RGCs, retinal Aβ and tau pathology, and RGC integrity was assessed, and correlations to disease status were determined. Our analyses indicated an early and substantial decrease in RGCs, concomitant with an increase in pS396-tau-laden RGCs in MCI and AD patients compared to age- and sex-matched CN controls. The levels of total retinal pS396-tau and pS396-

133 tau-laden RGCs correlated with the extent of RGC decline. RGCs in AD patients exhibited
134 hypertrophic soma and nucleus displacement. Notably, increased pS396-tau^{+} RGC counts strongly
135 correlated with corresponding brain pathology and cognitive status.

136

137 **Materials and Methods**

138 **Postmortem Eyes**. Human eye and brain tissues were collected from donor patients with
139 premortem clinical diagnoses of MCI and AD dementia (confirmed by postmortem AD
140 neuropathology), along with age- and sex-matched CN controls (total *n*=41 subjects). These tissues
141 were primarily obtained from the Alzheimer's Disease Research Center (ADRC) Neuropathology
142 Core in the Department of Pathology (IRB protocol HS-042071) at the Keck School of Medicine,
143 University of Southern California (USC, Los Angeles, CA). Additional eyes were obtained from
144 the National Disease Research Interchange (NDRI, Philadelphia, PA) under the approved Cedars-
145 Sinai Medical Center IRB protocol Pro00019393. Both USC-ADRC and NDRI maintain human
146 tissue collection protocols approved by their managerial committees and subject to oversight by
147 the National Institutes of Health. Histological studies at Cedars-Sinai Medical Center were
148 performed under IRB protocols Pro00053412 and Pro00019393. Demographic, clinical, and
149 neuropathological information on human donors is detailed in **Table 1 and Suppl**. **Table 1**.
150 Subjects with macular degeneration, glaucoma, and diabetic retinopathy were excluded from this
151 study. The available retinal tissues from individual donors are specified in **Suppl. Table 1**. For the
152 histopathological analysis, the human cohort consisted of AD dementia (n=15), MCI due to AD
153 (n=10), and CN controls (n=16). All patients' identities were protected by de-identifying tissue
154 samples, ensuring they could not be traced back to the donors.

155

Clinical and Neuropathological Assessments. The ADRC provided clinical and neuropathological reports on patients' neurological examinations, neuropsychological and cognitive tests, family history, and medication lists, as collected in the ADRC system using the Uniform Data Set (UDS) [12]. The NDRI provided the medical history of additional patients. Most cognitive evaluations were performed annually and, in most cases, less than one year prior to death. Cognitive testing scores from evaluations made closest to the patient's death were used for this analysis. Two global indicators of cognitive status were used for clinical assessment: the Clinical Dementia Rating (CDR scores: 0 = normal; 0.5 = very mild impairment; 1 = mild dementia; 2 = moderate dementia; or 3 = severe dementia) [82] and the Mini-Mental State Examination (MMSE scores: 24–30 = CN; 20–23 = MCI; 10–19 = moderate dementia; or 9 ≥ severe dementia) [34]. In this study, the composition of the clinical diagnostic groups (AD, MCI, or CN) was determined by source clinicians based on a comprehensive battery of tests, including neurological examinations, neuropsychological evaluations, and the cognitive tests. Specifically, the diagnosis of MCI due to AD was assigned to patients who had an antemortem clinical diagnosis of MCI (based on the comprehensive battery of behavioral and cognitive tests) caused by AD. These patients had a postmortem confirmation of AD neuropathology (according to the ADNC—Alzheimer's disease neuropathological change guidelines) and showed no evidence of other diseases, such as Lewy body dementia, Parkinson's disease, FTD/FTLD (PSP or Pick's disease), or cognitive impairment due to stroke or small vessel disease.

To obtain a final diagnosis based on the neuropathological reports, we used the modified Consortium to Establish a Registry for Alzheimer's Disease (CERAD) criteria [77, 99], as outlined in the National Institute on Aging (NIA)/Regan protocols with revisions by the NIA and Alzheimer's Association [49]. The assessment included Aβ burden (measured as diffuse,

immature, or mature plaques), amyloid angiopathy, neuritic plaques, NFTs, neuropil threads (NTs), granulovacuolar degeneration, Lewy bodies, Hirano bodies, Pick bodies, balloon cells, neuronal loss, microvascular changes, and gliosis. These pathologies were assessed in multiple brain areas, including the hippocampus (particularly the Cornu ammonis CA1, at the level of the thalamic lateral geniculate body), entorhinal cortex, superior frontal gyrus of the frontal lobe, superior temporal gyrus of the temporal lobe, superior parietal lobule of the parietal lobe, primary visual cortex (Brodmann Area-17), and visual association (Area-18) of the occipital lobe. In all cases, uniform brain sampling was conducted by a neuropathologist.

Cerebral amyloid plaques, NFTs, and NTs were evaluated using anti–β-amyloid mAb clone 4G8 immunostaining, Thioflavin-S (ThioS) histochemical staining, and Gallyas silver staining in formalin-fixed, paraffin-embedded tissue sections. The ADRC neuropathologists assigned severity scores based on semi-quantitative observations. The scale for Aβ/neuritic plaques was determined by the presence of 4G8- and/or Thioflavin-S-positive and/or Gallyas silver-positive plaques measured per 1 mm^2 of brain area (0 = none; 1 = sparse [≤ 5 plaques]; 3 = moderate [6–20 plaques]; 5 = abundant/frequent [21–30 plaques or greater]; or N/A = not applicable), as previously described [80] in the NACC NP Guidebook, Version 10, January 2014: https://naccdata.org/data-collection/forms-documentation/np-10. The brain NFT or NT severity scoring system was derived from observed burden of these AD neuropathologic changes, as detected by Gallyas silver and/or Thioflavin-S staining [79, 80, 119], and measured per 1 mm^2 of brain area. The assigned NFT or NT scores were as follows: 0 = none; 1 = sparse (mild burden); 3 = moderate (intermediate burden); or 5 = frequent (severe burden). For both histochemical and immunohistochemical staining, each anatomical area of interest was assessed for relevant pathology using a 20X objective (200X high power magnification), and representative fields were graded using the semiquantitative scale as

detailed above. Validation of AD neuropathic change (ADNC), especially NTs, was performed using a 40X objective (400X high power magnification), and an average of two readings was assigned to each individual patient.

A final diagnosis of AD neuropathological change was determined using an "ABC" score derived from three separate 4-point scales. We used the modified Aβ plaque Thal score (A0 = no Aβ or amyloid plaques; A1 = Thal phase 1 or 2; A2 = Thal phase 3; or A3 = Thal phase 4 or 5) [115]. For the NFT stage, we applied the modified Braak staging for silver-based histochemistry or p-tau IHC (B0 = no NFTs; B1 = Braak stage I or II; B2 = Braak stage III or IV; or B3 = Braak stage V or VI) [19]. For neuritic plaques, we used the modified CERAD score (C0 = no neuritic plaques; C1 = CERAD score sparse; C2 = CERAD score moderate; or C3 = CERAD score frequent) [77]. Neuronal loss, gliosis, granulovacuolar degeneration, Hirano bodies, Lewy bodies, Pick bodies, and balloon cells were all evaluated (0 = absent; 1 = present) in multiple brain areas by staining tissues with hematoxylin and eosin (H&E). Brain atrophy was evaluated (0 = none; 1 = mild; 3 = moderate; 5 = severe; or 9 = not applicable).

Processing of Eye Globes and Retinal Tissues. The processing of eye globes, isolation and preparation of retinal strips, and retinal immunostaining were extensively detailed in [60, 61, 108]. Briefly, donor eyes were collected within an average of 9 hours after death and subjected to the following preservation methods: 1) preserved in Optisol-GS media (Bausch & Lomb, 50006-OPT) and stored at 4°C for less than 24 hours, or 2) punctured once and fixed in 10% neutral buffered formalin (NBF) or 4% paraformaldehyde (PFA) and stored at 4°C. Regardless of the source of the human donor eye (USC-ADRC or NDRI), the same tissue collection and processing methods were applied.

Preparation of Retinal Strips. Eyes fixed in 10% NBF or 4% PFA were dissected as previously described [60, 61, 108]. Flatmounts were prepared after careful dissection of the eye globes and thorough cleaning of the vitreous humor. Flatmount strips (~2 mm wide) extending diagonally from the optic disc (OD) to the ora serrata (~20–25 mm long) were prepared in 4 predefined regions: Superior Temporal (ST), Inferior Temporal (IT), Inferior Nasal (IN), and Superior Nasal (SN). In this study, we focused our analysis on the ST retinal strip due to the high presence of AD pathology in this region [60, 61, 108]. The flatmount-derived strips were then paraffinized using standard techniques and embedded in paraffin after flip-rotating 90° horizontally. The retinal strips were sectioned (7-10 µm thick) and mounted on microscope slides coated with APES. This sample preparation technique allowed for extensive and consistent access to retinal quadrants, layers, and pathological subregions.

Immunofluorescent Staining. Retinal sections were deparaffinized using 100% xylene twice (10 minutes each), rehydrated with decreasing concentrations of ethanol (100% to 70%), and washed with distilled water followed by PBS. After deparaffinization, tissue sections were treated with target retrieval solution (pH 6.1; S1699, Dako) at 98°C for 1 hour and then washed with PBS. Next, tissues were incubated in blocking buffer (Dako #X0909) supplemented with 0.1% Triton X-100 (Sigma, T8787) for 1 hour at room temperature (RT), followed by overnight incubation with primary antibody (Ab) at 4°C (Abs information provided in **Suppl. Table 2**). The sections were then washed three times with PBS and incubated with secondary Abs against each species (1:200, **Suppl. Table 2**) for 1 hour at RT. After rinsing with PBS three times, the sections were mounted with ProLong Gold antifade reagent with DAPI (Thermo Fisher #P36935).

Peroxidase-based Immunostaining. After deparaffinization and antigen retrieval treatment, the tissues were treated with 70% formic acid (ACROS) for 10 minutes at room temperature. The

tissues were then washed with wash buffer (Dako S3006) supplemented with 0.1% Triton X-100 (Sigma, T8787) for 1 hour, followed by treatment with H_2O_2 for 10 minutes and a rinse with wash buffer. Primary Ab (**Suppl. Table 2**) were diluted with background reducing components (Dako S3022) and incubated with the tissues overnight at 4°C. The tissues were rinsed thrice with wash buffer on a shaker and incubated for 30 minutes at 37°C with secondary Ab (goat anti-rabbit HRP conjugated, Dako Envision K4003), followed by three more rinses with wash buffer on a shaker. Diaminobenzidine (DAB) substrate (Dako K3468) was then applied. Some slides were counterstained with hematoxylin and mounted with Faramount aqueous mounting medium (Dako, S3025). Routine controls were processed using an identical protocol, while omitting the primary antibodies to assess nonspecific labeling.

Nissl Staining. A basic (alkaline) dye was used to label nuclei and granules (i.e., ribosomal RNA) in neurons. The cytoplasm of neurons is specifically stained with the Nissl staining technique, while the perikarya of other cellular elements are either weakly visualized or not at all [52]. Deparaffinized and rehydrated sections were stained in 0.1% Cresyl Violet acetate (Sigma #C5042) for 5 min, rapidly rinsed in tap water, and briefly dipped in 70% ethanol. The sections were then dehydrated through 2 changes of absolute ethanol for 3 minutes each, followed by immersion in xylene twice for 2 minutes and mounted in mounting medium xylene (Fisher scientific company, L.L.C. #245-691). An average of 12 images (from the superior quadrant), covering the retinal neurons from the optic disc to the ora serrata, were captured at a 20x objective and analyzed to quantify the area and number of retinal GCL neurons.

Microscopy and Stereological Quantification. Fluorescence and brightfield images were acquired using a Carl Zeiss Axio Imager Z1 fluorescence microscope (with motorized Z-drive) equipped with ApoTome, AxioCam HRc, and AxioCam MRm monochrome cameras (version 3.0;

resolution of 1388 × 1040 pixels, 6.45 µm × 6.45 µm pixel size, and a dynamic range of >1:2200, which delivers low-noise images due to a Peltier-cooled sensor) with ZEN 2.6 blue edition software (Carl Zeiss MicroImaging, Inc.). Multi-channel image acquisition was used to create images with multiple channels. Images were consistently captured at the same focal planes with identical exposure time, using a 20x objective at a resolution of 0.25 µm. Approximately 15 images were obtained from each retina. The acquired images were converted to grayscale and standardized to baseline using a histogram-based threshold in Fiji ImageJ (NIH) software (version 1.53c). For each biomarker, the total area of immunoreactivity was determined using the same threshold percentage from the baseline in ImageJ (with the same percentage threshold setting for all diagnostic groups). The images were then subjected to particle analysis to determine the immunoreactive (IR) area and/or area fraction (%).

RGC Soma Size Measurement. The size of RGC somas was measured using Fiji ImageJ (NIH) software (version 1.53c) with the polygonal selection tool. For each 20x retinal image, the soma area of up to three cells was manually assessed, focusing on the three largest cells in each field. The average soma area for each subject was then computed, followed by statistical analysis. On average, 30 somas were analyzed per patient, with a total of 542 somas measured.

Statistical Analysis. GraphPad Prism Software version 9.5.1 was used for statistical analyses. One-way or two-way ANOVA followed by Tukey's multiple comparison post-test was used to determine statistical significance between three or more groups. Two-group comparisons were analyzed using a two-tailed unpaired Student's *t-test*. The statistical association between two or more Gaussian-distributed variables was determined by Pearson's correlation coefficient (*r*) test. Scatterplot graphs present the null hypothesis of pair-wise Pearson's *r*, with unadjusted P values indicating the direction and strength of the linear relationship between two variables. Results are

293 expressed as the mean ± standard deviation (SD) in tables and as median, lower, and upper
294 quartiles in violin plots. Degrees of significance are presented as: *P < 0.05, **P < 0.01,
295 ***P < 0.001, and ****P < 0.0001. Data analysis was conducted using coded identifiers, and
296 analysts remained blinded to the diagnostic groups until all analyses were completed.

297

298 **Results**

299 To investigate the integrity of RGCs, including their number, morphology, and distribution in
300 relation to abnormal retinal tau isoforms and their accumulation within RGCs in early and
301 advanced-stage AD, we selected and analyzed retinal superior temporal (ST) cross-sections (**Fig.**
302 **1a, b**) from patients with MCI due to AD (n=10, mean age 88.4 ± 6.6 years, 7 females/3 males)
303 and AD dementia (n=15, mean age 87.5 ± 8.0 years, 8 females/7 males), compared to CN controls
304 (n=16, mean age 80.5 ± 11.1 years, 10 females/6 males). Demographic, clinical, and
305 neuropathological information are detailed in **Table 1** (list of individual donor eyes and respective
306 brains detailed in **Suppl. Table 1**).

307 **1. Severe RGC decline in MCI and AD patients.**

308 We first assessed RGC numbers and distribution across ST subregions in a sub-cohort of patients
309 with MCI (n=6, mean age 89.5 ± 5.24 years, 3 females/3 males), AD (n=10, mean age 86.0 ± 8.89
310 years, 4 females/6 males), and age- and sex-matched CN controls (n=9, mean age 85.89 ± 11.85
311 years, 5 females/4 males), using a selective pan-RGC marker, ribonucleic acid binding protein
312 with multiple splicing (RBPMS), for immunohistochemical (IHC) analysis. According to previous
313 studies, RBPMS is specifically expressed in the entire RGC population, despite the heterogeneity
314 of other neurons under pathological conditions, including displaced amacrine cells within the GCL
315 [88, 91, 98]. In comparison to the retinas of CN individuals, the density of RGCs was lower in

MCI and AD dementia patients, with their cytoplasm appearing enlarged or swollen (**Fig. 1c** and **Suppl. Figure 1a**). Analysis of $RBPMS^+$ RGC cell counts per retinal subregion (central, mid-, and far-periphery) and the total ST region revealed substantial reductions in RGC count and percent area–ranging from 42% to 65%–in MCI and AD patients compared to CN individuals (**Fig. 1d, e** and **Suppl. Fig. 1b**; P<0.05-0.01). RGC loss in MCI and AD retinas appeared more extensive in the mid- and far-periphery regions, which are further distal from the optic nerve head.

We next examined neurodegeneration in the GCL using histological Nissl staining, an alkaline dye that labels nuclei and granules (i.e., ribosomal RNA) in neurons, in a sub-cohort of patients diagnosed with MCI (n=10, mean age 88.4 ± 6.6 years, 7 females/3 males), AD (n=15, mean age 87.5 ± 8.0 years, 8 females/7 males), and CN controls (n=14, mean age 80.6 ± 12.1 years, 9 females/5 males) (**Fig. 1f-i**). Representative images showed a reduction in cells numbers across all retinal layers (**Fig. 1f**), particularly in the GCL (**Fig. 1g**), in MCI and AD patients compared to CN controls. Quantitative analysis of $Nissl^+$ percent area in the GCL across retinal subregions indicated a marked 53%-64% neuronal loss in the central and mid-peripheral subregions of MCI and AD patients compared to CN controls (**Fig. 1h**); no statistically significant reduction was observed in the far-peripheral subregion. In the total ST region, a substantial 55%-56% reduction in $Nissl^+$ percent area in the GCL was observed for both AD and MCI groups compared to CN controls (**Fig. 1i**; P<0.01-0.001). Pearson's correlation coefficient (*r*) analysis demonstrated a strong correlation between the two RGC integrity parameters, $RBPMS^+$ RGCs and $Nissl^+$ neurons in the GCL (r=0.63, P=0.0011; **Fig. 1j**). To assess whether GCL residing neurons were lost due to apoptotic cell death mechanisms, we performed IHC using an antibody against cleaved caspase 3 (CCasp3), an early apoptotic marker [117]. Analysis of the percent of $CCasp3^+$ cells in the GCL revealed a significant 1.5-fold and 1.3-fold increase in AD retinas compared to CN and MCI retinas,

respectively (**Fig. 1k**; P<0.05-0.01), with no differences noted between the MCI and CN retinas. When the CCasp3^{+} cell immunoreactive area in the total retina was normalized to retinal thickness, there were highly significant 3.1-fold and 2-fold increases in AD compared to CN and MCI, respectively (P<0.001-0.0001), with a trend toward a 1.5-fold increase in MCI compared to CN, reaching significance by Student's *t*-test (**Suppl. Fig. 1c**).

2. Increased pS396-tau laden RGCs of MCI and AD patients is linked to RGC hypertrophy and loss.

We recently found significant increases in AD-related tau isoforms, particularly pretangles such as pS396-tau and tau oligomers (oligo-tau), in the retinas of MCI and AD patients, which strongly correlated with corresponding brain pathology and cognitive deficits [108]. In this study, we investigated whether RGCs are vulnerable to these tau isoforms in early and advanced AD (**Fig. 2**; extended data in **Suppl. Fig. 2**). Utilizing the same sub-cohort of patients outlined above for the RBPMS analysis, we performed an IHC analysis employing a combination of RBPMS and pS396-tau, which recognizes the hyperphosphorylated tau protein at serine residue 396 in the C-terminal region. Representative microscopic images depicted increases in pS396-tau burden within the OPL, IPL, GCL, and NFL, along with cell swelling (hypertrophic soma), whereas a reduction in the number of RBPMS^{+} RGC was observed in MCI and AD patients was seen compared to CN controls (**Fig. 2a)**. The three-parallel-string staining pattern of retinal pS396-tau in the IPL of MCI and AD patients appeared to accumulate in neuronal dendrites of RGCs connecting with axons of bipolar and amacrine cells. Notably, morphological changes were observed in the RGCs of MCI and AD patients compared to CN controls (**Fig. 2a-d** and **Suppl. Fig. 2a, b**). These ganglion cells exhibited granulovacuolar vesicles degeneration (GVD)-like bodies and nucleus displacement, as indicated by white and red arrows, respectively (**Fig. 2b** and **Suppl. Fig. 2a**). Analysis of the

enlarged and granulomatous soma areas of RBPMS$^+$ RGCs revealed a significant 1.5-fold increase in RGC soma size in AD patients compared to CN controls (P=0.018), with no difference observed in RGC size in MCI patients (**Fig. 2b'**).

To assess whether p-tau inclusions exist and increase within RGCs of MCI and AD patients, we next immunolabeled retinal cross-sections for pS396-tau in combination with RBPMS and parvalbumin, the latter being a marker of horizontal cells within the OPL and RGCs [57]. Our analysis identified pS396-tau accumulation within hypertrophic RBPMS$^+$ RGCs and horizontal cells of MCI and AD patients, and occasionally in RBPMS$^+$ RGCs of CN individuals (**Fig. 2c, d** and **Suppl. Fig. 2b**). Moreover, pS396-tau build-up within the somas of RGCs in the GCL was evident in non-fluorescence, peroxidase-based IHC staining (**Fig. 2e,** red arrows**)**. Quantitative analysis of retinal cross-sections in this cohort showed a highly significant 2.4-fold increase in total pS396-tau$^+$ % area in MCI and AD patients compared to CN controls (**Suppl. Fig. 2c**; p<0.0001). Importantly, compared to the CN retina, pS396-tau-positive RBPMS$^+$ RGC counts were significantly increased in MCI (2.1-2.3-fold; P<0.05-0.01), and AD (2.9-4.1-fold; P<0.01-0.0001) retinas when analyzed per retinal subregion and in the total ST region (**Fig. 2f, g**). Increases in the pS396-tau$^+$ RBPMS$^+$ RGC count, as well as the percentage area of pS396-tau$^+$ in the GCL of MCI and AD patients, were more significant in the central ST retina (**Fig. 2f** and **Suppl. Fig. 2d, e**). Additional analysis of T22$^+$ oligo-tau in the retinas of MCI and AD patients compared to CN controls identified oligo-tau aggregates within swollen RGCs of the GCL (**Fig. 2h** and **Suppl. Fig. 2f**).

To investigate the interrelations between pS396-tau-containing RBPMS$^+$ RGCs, retinal pS396-tau, retinal Aβ burden, retinal oligo-tau, and RGC loss, we applied Pearson's correlation coefficient (*r*) analyses (**Fig. 2i-m** and **Suppl. Fig. 2g-j**) in our cohort. As expected, we found a strong positive

correlation between retinal pS396-tau burden and the number of pS396-tau$^+$ RBPMS$^+$ RGCs (**Suppl. Fig. 2g**; r=0.72 and P<0.0001). An unexpected strong correlation was detected between retinal Aβ_{42} burden and pS396-tau$^+$ RBPMS$^+$ RGC number (**Suppl. Fig. 2h**; r=0.69 and P=0.003). We then assessed whether there was a connection between the presence of pS396-tau in RBPMS$^+$ RGCs, RGC loss, and the level of CCasp3$^+$ in the GCL. Pearson's correlation analyses revealed moderate associations between pS396-tau$^+$ RBPMS$^+$ RGCs and GCL Nissl$^+$ cells (**Fig. 2i**; r=-0.53 and P=0.0091), or RBPMS$^+$ RGCs (**Fig. 2j**; r=-0.40 and P=0.049). Notably, the apoptotic marker CCasp3$^+$ cells in the GCL strongly correlated with pS396-tau$^+$ RBPMS$^+$ RGCs (**Suppl. Fig. 2i**; r=0.66 and P=0.036). We next assessed the relationship between overall retinal pS396-tau$^+$, retinal Aβ_{42}, retinal intra-RGC Aβ oligomers, and retinal oligo-tau burdens and RGC integrity. Pearson's correlation analyses revealed moderate to strong correlations between retinal pS396-tau$^+$ (**Fig. 2k**; r=-0.60 and P=0.0017), retinal 12F4$^+$-Aβ_{42} (**Suppl. Fig. 2l**; r=-0.53 and P=0.033), retinal scFvA13$^+$Aβ oligomers in RGCs (**Fig. 2l**; r=-0.74 and P=0.0022), and retinal T22$^+$ tau oligomers (**Fig. 2m** r=-0.64, P=0.002), with RGC reduction.

3. Retinal p-tau-containing ganglion cells correlate with AD status.

We further tested the potential relationship between pS396-tau$^+$ RBPMS$^+$ RGCs or diminished RGCs and the severity of brain pathology and cognitive deficits (**Fig. 3**, **Tables 2-3**; extended data in **Suppl. Fig. 3**). Pearson's correlation coefficient (r) analyses revealed that pS396-tau$^+$ RGC count strongly associated with brain Aβ-plaque and NFT severity scores (**Fig. 3a, b**; r=0.62, P=0.0017 and r=0.71, P=0.0001, respectively). Stratifying patients based on Braak stage severity showed significant 1.9-2.7-fold increases in pS396-tau$^+$ RBPMS$^+$ RGCs in the high (V-VI) and, to a lesser extent, the intermediate (III-IV) Braak stage groups compared to the low (0-II) group (**Fig. 3c**; P=0.0033 and P=0.042, respectively). The pS396-tau$^+$ RBPMS$^+$ RGCs were strongly correlated

with Braak stage (**Fig. 3d**; r=0.65, P=0.0009), while no correlation was detected between RBPMS$^+$ RGC count and Braak stage (**Suppl. Fig. 3a**). Similarly, pS396-tau$^+$ RBPMS$^+$ RGC counts were strongly correlated with disease severity ABC scores (**Fig. 3e**; r=0.65, P=0.0007), as well as with the cerebral amyloid angiopathy (CAA) grades (**Fig. 3f**; r=0.63, P=0.0014). Moderate inverse correlations were detected between GCL Nissl$^+$ neuronal % area or RBPMS$^+$ RGC counts and CAA grades (**Suppl. Fig. 3b, c**; r=-0.42, P=0.06 and r=-0.54, P=0.011, respectively).

Finally, we assessed the potential associations between pS396-tau$^+$ RBPMS$^+$ RGC or RBPMS$^+$ RGC counts and cognitive status**.** Stratification of patients based on their clinical dementia rating (CDR) group revealed a significant 2.2-fold increase in pS396-tau$^+$ RGCs in the CDR 3 score group compared to the CDR 0-0.5 group (**Fig. 3g**; P=0.03), with a strong correlation between pS396-tau$^+$ RBPMS$^+$ RGC count and CDR score (**Fig. 3h**; r=0.60, P=0.0031). A moderate correlation was observed between RBPMS$^+$ RGC count and CDR score (**Suppl. Fig. 3d;** r=-0.49 and P=0.022). Importantly, stratifying patients based on the mini-mental state examination (MMSE) cut-off score of 26, which has been reported to have high sensitivity and specificity for detecting dementia [87], was utilized in our cohort. This analysis showed a significant 2-fold increase in pS396-tau$^+$ RBPMS$^+$ RGC counts in the MMSE ≤ 26 group compared to the MMSE >26 group (**Fig. 3i**; P=0.0059). Whereas no significant association was detected between RBPMS$^+$ RGC counts and MMSE score (**Suppl. Fig. 2e**), a highly significant and strong association was observed between pS396-tau$^+$ RBPMS$^+$ RGC count and MMSE score (**Fig. 3k**; r=-0.76, P=0.0004).

Discussion

In this study, we present the first evidence of abnormal tau inclusions within RBPMS-positive RGCs, concomitant with ganglion cell loss in the retinas of donor patients with MCI (due to AD) and AD dementia. Increases in pS396-tau-containing RBPMS-positive RGCs in both MCI and AD patients were accompanied by elevated apoptotic cell markers, necroptotic-like morphological changes in RGCs, including hypertrophic soma and nuclei displacement, and decreased RGC counts. Tau oligomers were also detected in swollen RGCs within the GCL. Notably, we found moderate to strong associations between RGC loss and pS396-tau burden in both RGCs and the retina as a whole. Moreover, we observed that retinal tau oligomers, as well as retinal $A\beta_{42}$ and intra-RGC Aβ oligomers, were strongly associated with RGC reduction, suggesting a link between retinal tau and amyloid pathologies and ganglion cell degeneration in AD. Importantly, our data indicated tight correlations between pS396-tau-containing $RBPMS^+$ RGCs and the respective brain pathology, disease stage, and cognitive status. Overall, our findings suggest that abnormal tau isoforms accumulate within $RBPMS^+$ RGCs and are associated with early and marked RGC loss in AD patients.

Among the RGC populations, the midget cells projecting to the parvocellular (P-cell) layers of the lateral geniculate nucleus (LGN) and the parasol cells projecting to the magnocellular (M-cell) layers of the LGN serve as two distinct visual pathways that process color and low spatial frequency contrast vision, respectively [69]. In AD patients, abnormalities in color vision, eye movement, contrast sensitivity, and visual integration have been detected early in disease progression [37, 47, 78] [32, 72, 101]. Therefore, fluctuations in color perception and abnormal contrast sensitivity in AD patients may be attributed to damage and loss of these RGC types, in addition to the involvement of horizontal and amacrine neurons. Here, the analysis of the RBPMS marker, a conserved RNA binding protein with a single RNA recognition motif expressed in RGCs

of humans and animal models [84, 91], facilitates differentiation from other retinal cells [63, 92, 98] and further validates our findings in RGCs. Notably, our analysis of RGC integrity in the superior temporal retina indicates marked decreases in $RBPMS^+$ RGC counts or immunoreactive area (by 47-55% in MCI and 46-50% in AD) compared to CN controls, with similar degrees of decreases observed in GCL $Nissl^+$ neurons (by 56% in MCI and 55% in AD patients). These results are consistent with previous studies reporting significant reductions in RGCs and the GCL in AD patients versus control subjects [6, 15-17] [101].

Specifically, the $RBPMS^+$ RGC count per retinal subregion indicated a 46% loss in MCI and a 57% loss in AD in the mid-periphery, as well as a 62% loss in MCI and a 45% loss in AD in the far periphery. Similarly, a study by Blanks et al., described GCL neuronal loss in AD as most pronounced in the superior and inferior quadrants, ranging between 40% and 49% throughout the mid-peripheral subregions and reaching 50-59% in the far-peripheral retina of AD patients [16]. These peripheral retinal subregions, which have anatomically fewer ganglion cells and a thinner nerve fiber layer, appear more vulnerable to RGC loss in AD, potentially due to a higher density of abnormal Aβ and tau species (e.g., $Aβ_{42}$, Aβ oligomers, PHF-tau, pS396-tau and p-tau (S202/T205)), and microgliosis [60, 61, 70, 108]. Interestingly, whereas the total and mid-peripheral ST retina consistently demonstrated significant and similar RGC reductions in both MCI and AD patients, as shown by the GCL $Nissl^+$ area and $RBPMS^+$ RGC count analyses, non-significant trends were noted for the far and central subregions, respectively. These differences may be due to variations in the types of analysis and staining patterns. The loss of RGCs in MCI and AD patients may explain previous reports of visual dysfunctions in AD, specifically impaired color and low spatial frequency contrast vision, as well as motion perception that can be attributed, at least in part, to the loss of M-cell and P-cell RGCs. In addition, a previous study of postmortem

476 AD retinas identified a reduction in melanopsin retinal ganglion cells (mRGCs), intrinsically
477 photosensitive cells that contribute to the photoentrainment of circadian rhythms, potentially
478 explaining the sleep disturbances observed in these patients [67].

479 In the brains of AD patients, the increase in hyperphosphorylated tau isoforms has been shown to
480 lead to tau aggregation, oligomerization, propagation, and NFT formation, ultimately causing
481 neuronal dysfunction and degeneration [90, 114]. Previous studies detected intracellular pretangles
482 and mature tangles in the retinas of AD patients [27, 29, 40, 45, 46, 60, 86, 108, 122]. Recently,
483 we also identified tau oligomers and citrullinated-tau, along with other tau isoforms, in the retinas
484 of MCI and AD patients. Notably, both pS396-tau and oligomeric-tau forms were frequently
485 observed within the GCL, with significant increases in MCI and AD patients [108]. The pS396-
486 tau isoform is increased in the AD brains and is linked to neuronal cell loss and Braak stage severity
487 [8, 36, 96, 120]. Here, we found a specific build-up of these pathological tau isoforms within RGCs
488 of MCI and AD patients, demonstrating their connection with RGC integrity, entailing similar
489 links to neurodegeneration and tauopathy as seen in the brain.

490 In this study, we detected higher numbers of $RBPMS^+$ RGCs containing pS396-tau in patients with
491 AD dementia and those at the earliest stages of functional impairment (MCI due to AD). The level
492 of pS396-tau in RGCs was even higher in AD patients compared to MCI patients, suggesting that
493 more RGCs are affected by pS396-tau as the disease progresses. Our data on pS396-tau^+ RGC
494 counts per retinal subregion indicated that the most significant and substantial changes were
495 detected in the central subregion across all analyzed groups, with less pronounced changes in the
496 mid-periphery and the far periphery. This could be attributed to the density of RGCs in each
497 subregion, as there are up to eight layers of ganglion cells in the central subregion and only one or
498 two layers with space between them in the far periphery [55]. Hence, there is a higher probability

that RGCs in the central subregion are impacted by pS396-tau compared to those in the peripheral subregions. These findings may guide potential future in vivo imaging of pS396-tau-positive RGCs in the central ST retina for early AD detection and monitoring of disease progression.

In both fluorescent and peroxidase-based staining methods, we observed a three-parallel-string staining pattern of retinal pS396-tau in the IPL of MCI and AD patients. Consistent with retinal neuroanatomy, these findings suggest that pS396-tau accumulates within the neuronal dendrites of RGCs, which connect with the axons of bipolar and amacrine cells. These tau aggregates in synaptic-rich regions may interfere with information transmission and could help explain the decrease in contrast sensitivity observed in MCI and AD patients. Moreover, in MCI and AD patients, the pS396-tau isoform was also observed in the OPL, specifically in horizontal cells. A recent study suggested that pS202/T205-tau ($AT8^{+}$) spreads from the OPL to the IPL/GCL in the AD retina [122]. The patterns of retinal pS396-tau burden in the NFL of CN subjects and the IPL/OPL of MCI and AD patients merit further investigation to understand how pS396-tau spreads across retinal layers and neuronal processes during AD progression.

Our analysis showed a moderate inverse correlation between pS396-tau^{+} RGCs and RGC integrity, and a stronger negative correlation between overall retinal pS396-tau burden and RGC integrity, suggesting that the extent of retinal pS396-tau load, including in neuronal dendrites connecting with RGCs, may have additive effects on RGC susceptibility. Beyond retinal p-tau, the strong negative associations of Aβ oligomers in RGCs and retinal tau oligomers with RGC reduction suggest their substantial and detrimental effects on RGC degeneration. These retinal findings in AD are consistent with similar reports connecting elevated Aβ and tau oligomers with neuronal loss in AD brains [3, 9, 68, 83, 105, 116]. As expected, the overall burden of retinal pS396-tau strongly correlated with the extent of pS396-tau-loaded RGCs. Unexpectedly, the levels of retinal

522 $A\beta_{42}$ also strongly correlated with the extent of RGC containing pS396-tau, suggesting that retinal
523 Aβ may be a driver of tauopathy in RGCs, similar to the interactions between Aβ and the spread
524 of tau in neurons of AD brains [18, 126].

525 Levels of the early apoptotic marker, cleaved caspase 3 [117], have been shown to be elevated in
526 AD brains, with a high degree of colocalization to neurofibrillary tangles within neurons [38, 112].
527 In the current study, we observed increased cleaved caspase 3 expression in GCL cells in AD, but
528 not MCI, patients compared to cognitively normal controls. This is consistent with previous studies
529 showing cleaved caspase 3^+/Tuj1^+ RGCs [40] and overall retinal cleaved caspase 3 expression [61]
530 in AD patients compared to controls. The elevated expression of retinal cleaved caspase 3 in GCL
531 cells, along with strong correlations with pS396-tau-loaded RGCs, suggests that pS396-tau may
532 trigger apoptotic cell death in RGCs.

533 RGCs are highly diverse, consisting of multiple subtypes that exhibit a range of morphological
534 and physiological characteristics, including variations in soma and cell body size [55]. In this
535 study, we observed that RGCs in aged CN individuals predominantly appear to have small-sized
536 somas, with a minority of cells exhibiting large and round somas. In contrast, a substantial number
537 of RGCs in MCI and AD patients appeared swollen, with enlarged somas, granulovacuolar-like
538 bodies, and displaced nuclei, particularly in those containing pS396-tau inclusions. To the best of
539 our knowledge, this is the first demonstration of hypertrophic RGCs in MCI and AD patients. This
540 abnormal RGC morphology is characteristic of neurons exhibiting granulovacuolar degeneration
541 due to necroptosis, a process observed in the brains of individuals with preclinical AD and AD
542 dementia [59]. The morphology and process of necroptotic cells are characterized by compromised
543 plasma membrane integrity, organelle and cell enlargement, chromatin fragmentation, and
544 eventual cell lysis [89, 125]. Moreover, studies have indicated that necroptosis is involved in AD

brain pathology and is closely linked to tau pathology and Braak stage progression [11, 21, 59], with recent research showing that p-tau contributes to neuronal death by inducing necroptosis and inflammation [28]. In this study, the abnormal morphology of RGCs, particularly in those with a pS396-tau burden, may indicate necroptotic cell death in the RGCs of AD retinas. Future studies are needed to determine the potential role of p-tau in retinal ganglion cell death in AD.

Looking into the potential connections between pS396-tau-containing RGCs and disease status, our analysis indicates strong associations between pS396-tau^{+} RGCs and the following brain pathologies: Aβ plaques, NFTs, Braak stage, and ABC neuropathic changes. However, RGC counts alone did not correlate with these AD brain parameters. These data suggest that tauopathy-laden RGCs (measured here by RBPMS^{+} RGCs with a pS396-tau burden) may represent the link between retinal neuronal injury and brain AD pathology and disease progression. The strong correlation between pS396-tau-positive RGCs and CAA severity may simply reflect brain Aβ burden, as CAA involves cerebrovascular deposition of Aβ and is influenced by Aβ plaque levels [39]. In our cohort, pS396-tau-containing RGCs had comparable correlations with brain Aβ plaques and CAA severity. Importantly, our data indicate that pS396-tau-containing RGC numbers strongly correlate with cognitive status, as measured by the CDR, and even more so with MMSE scores. While the CDR is a test that allows assessment of cognitive, behavioral, and functional performance associated with AD, the MMSE test evaluates cerebral competency, comprehension, and communication. Our findings suggest that a future retinal imaging approach that reliably measures the number of RGCs containing pS396-tau in the ST central region holds potential as a marker to evaluate brain NFT severity, Braak staging, ABC scores, and cognitive deficits in AD patients. In the clinical setting, GCL layer is assessed by OCT [37, 73, 75, 109], apoptotic RGCs can be images by detection of apoptosing retinal cells (DARK) method [10, 26], and more specific

RGC changes could be detectable in the inner retina using high resolution imaging systems, such as AO-OCT. Imaging RGCs, combined with future p-tau tracers, could serve as a non-invasive biomarker for early AD diagnosis and monitoring of disease progression. This would be immensely valuable in future trials evaluating new treatments for AD.

We acknowledge several limitations of this study. As a cross-sectional, case-control study, our focus was primarily on group stratification and correlations, so caution must be exercised before implicating cause-and-effect conclusions. Moreover, the lack of clinical information on visual system-related symptoms hinders our ability to assess potential connections between pS396-tau$^+$ RBPMS$^+$ RGCs and various manifestations of visual dysfunction. This highlights the need for future studies to explore the relationships between pS396-tau$^+$ RGCs, RGC loss, and ocular outcomes in patients. Future studies in larger and more diverse populations are warranted to validate these findings and to compare RGC susceptibility with that of other retinal cell types in relation to AD processes.

Conclusion

In summary, this study provides the first evidence of RGCs laden with abnormal tau inclusions, pS396-tau and oligomeric tau, in early (MCI) and advanced-stage AD patients, with clear indications of increased RGC vulnerability. RBPMS-positive RGCs containing pS396-tau correlated with increased apoptotic markers, necroptotic-like morphological changes, and reduced RGC counts, suggesting that these tau pathologies may contribute to ganglion cell degeneration in AD. Notably, strong correlations were found between pS396-tau laden RGCs and brain AD pathology, cognitive status, and disease stage. This study highlights the potential of imaging tau-

laden RGCs as a non-invasive biomarker for early AD diagnosis and monitoring disease progression. However, further research is needed to more definitively establish these connections.

Abbreviations:

A – Amyloid; Ab – Antibody; ABC – Amyloid/Braak/CERAD score; AD – Alzheimer's disease; ADRC –Alzheimer's disease research center; Aβ – Amyloid β-protein; ANOVA – Analysis of variance; B – Brain; C – Central retina; CCasp3 – Cleaved caspase 3; CDR – Clinical Dementia Rating; CN – Cognitively normal; F – Far-peripheral retina; GCL – Ganglion cell layer; IHC – Immunohistochemistry; INL – Inner nuclear layer; IPL – Inner plexiform layer; IR area – Immunoreactive area; mAb – Monoclonal antibody; M – Middle-peripheral retina; MCI – Mild Cognitive Impairment; MMSE – Mini-mental state examination; mRGC – Melanopsin Retinal Ganglion Cell; NDRI – National disease research interchange; NFL – Nerve fiber layer; NFT – Neurofibrillary tangle; NT – Neuropil thread; OD – Optic disc; ONL – Outer nuclear layer; OPL – Outer plexiform layer; pAb – Polyclonal antibody; PMI – Postmortem interval; p-tau – Hyperphosphorylated tau; RBPMS – Ribonucleic acid binding protein with multiple splicing; RGC – Retinal Ganglion Cell(s); Serine 396 – S396; SD – Standard deviation; ST – Superior temporal.

Table 1. Demographic and neuropathological data on human brain and retinal donors in this study.

		CN	MCI	AD	*F*	P
Retinal samples (N = 41)		16 10F (63%) 6M	10 7F (70%) 3M	15 8F (53%) 7M	-	-
Age at death (years)		80.5 ± 11.1	88.4 ± 6.6	87.5 ± 8.0	2.93	0.07
Race		14W, 1H, 1B	8W, 1B, 1H	12W, 2H, 1A	-	-
PMI (h)		7.8 ± 4.5	10.1 ± 5.4	8.8 ± 4.5	0.5	0.73
MMSE score (N=30)		28.7 ± 2.1	20.1 ± 7.0	13.8 ± 7.3	17.01	**<0.0001**
CDR score (N=31)		0.57 ± 0.8	2.1 ± 1.1	2.5 ± 0.9	10.53	**0.0004**
Brain neuropathology (N=32)	Braak stage (%)	0-II (57%) III-IV (43%) V-VI (0%)	0-II (30%) III-IV (30%) V-VI (40%)	0-II (0%) III-IV (13%) V-VI (87%)	15.2	**<0.0001**
	ABC average	1.37 ± 0.91	2.20 ± 0.59	2.82 ± 0.21	17.13	**<0.0001**
	Aβ plaque (severity score)	1.12 ± 1.31	1.88 ± 0.79	2.65 ± 0.77	6.98	**0.0034**
	NFTs (severity score)	0.43 ± 0.53	1.71 ± 0.91	2.36 ± 0.70	16.06	**<0.0001**
	NTs (severity score)	0.49 ± 0.99	1.24 ± 0.82	1.69 ± 0.90	4.27	**0.024**

List of human donors included in this study (N = 41 subjects). Paired brains with neuropathological assessments were available for 32 human donors. ABC scores comprise of mean grades for: (A) Aβ plaque score modified from Thal, (B) NFT stage modified from Braak, and (C) neuritic plaque score modified from CERAD. Group values are presented as mean ± standard deviation. *F* and P-values were determined using one-way analysis of variance (ANOVA) with Tukey's multiple comparisons test. P-values presented in bold type demonstrate statistical significance. Abbreviations: Aβ, amyloid beta-protein; AD, Alzheimer's disease; A, Asian; B, Black; CDR, Clinical Dementia Rating; CN, cognitively normal controls; F, female; H, Hispanic; M, male; MCI, mild cognitive impairment; MMSE, Mini-Mental State Examination; NFTs, neurofibrillary tangles; NTs, neuropil threads; PMI, postmortem interval; W, White.

624 **Table 2**. Correlations between RGC parameters and brain pathology.

	Aβ (severity score)		**CAA (grade)**		**NFT (severity score)**		**BRAAK (stage)**		**ABC (score)**	
	N = 17-23		N = 17-23		N = 17-23		N = 17-23		N = 17-23	
	r	P	*r*	P	*r*	P	*r*	P	*r*	P
RBPMS$^+$ RGCs (count)										
Total	-0.22	0.32	-0.26	0.23	-0.29	0.18	-0.15	0.50	-0.19	0.38
Central	-0.18	0.47	-0.35	0.16	-0.27	0.28	-0.14	0.57	-0.23	0.35
Mid-periphery	-0.29	0.20	**-0.54**	**0.011***	-0.38	0.091	-0.27	0.24	-0.32	0.16
Far-periphery	-0.18	0.41	-0.30	0.17	-0.29	0.17	-0.20	0.35	-0.17	0.43
Nissl$^+$ in GCL (% area)										
Total	-0.11	0.64	**-0.42**	**0.060***	-0.094	0.69	-0.088	0.70	-0.07	0.76
Central	-0.16	0.55	**-0.49**	**0.045***	-0.22	0.40	-0.28	0.28	-0.24	0.35
Mid-periphery	0.022	0.93	**-0.48**	**0.028***	-0.10	0.66	-0.12	0.60	-0.024	0.92
Far-periphery	-0.31	0.19	-0.42	0.065	-0.030	0.90	0.043	0.86	-0.17	0.46
pS396-tau$^+$ in RGCs (count)										
Total	**0.62**	**0.0017****	**0.63**	**0.0014****	**0.71**	**0.00010*****	**0.65**	**0.0009*****	**0.65**	**0.0007*****
Central	**0.65**	**0.0038****	**0.59**	**0.010***	**0.70**	**0.0014****	**0.68**	**0.0019****	**0.67**	**0.0023****
Mid-periphery	**0.51**	**0.017***	**0.56**	**0.009****	**0.72**	**0.00020*****	**0.62**	**0.0029****	**0.57**	**0.0073****
Far-periphery	**0.59**	**0.0029****	**0.53**	**0.009****	**0.71**	**0.00020*****	**0.63**	**0.0012****	**0.66**	**0.00070*****

625 Pearson's correlation analyses: P and *r*-values determine the statistical significance and strength
626 of each pairwise association between retinal RGC marker and brain pathology. P and *r*-values
627 presented in bold type with asterisk(s) are statistically significant (<0.05). Aβ, amyloid beta-
628 protein; CAA, cerebral amyloid angiopathy; NFTs, neurofibrillary tangles. ABC scores comprise
629 of mean grades for: (A) Aβ plaque score modified from Thal, (B) NFT stage modified from Braak,
630 and (C) neuritic plaque score modified from CERAD.
631

632 **Table 3**. Correlations between RGC parameters and the cognitive status.

633

	CDR (score)		**MMSE (score)**	
	N = 16-22		N = 15-18	
	r	P	*r*	P
RBPMS$^+$ RGCs (count)				
Total	-0.39	0.070	0.42	0.097
Central	-0.11	0.67	0.36	0.19
Mid-periphery	**-0.45**	**0.047***	**0.48**	**0.050**
Far- periphery	**-0.49**	**0.022***	0.42	0.094
Nissl$^+$ in GCL (% area)				
Total	-0.40	0.080	0.33	0.24
Central	**-0.56**	**0.023***	0.31	0.31
Mid-periphery	-0.35	0.13	0.38	0.16
Far-periphery	-0.26	0.29	0.43	0.11
pS396-tau$^+$ in RGCs (count)				
Total	**0.60**	**0.0031****	**-0.76**	**0.00040*****
Central	**0.65**	**0.0049****	**-0.74**	**0.0018****
Mid-periphery	**0.62**	**0.0037****	**-0.71**	**0.0016****
Far-periphery	**0.61**	**0.0023****	**-0.59**	**0.0013****

634 Pearson's correlation analyses: P and *r*-values determine the statistical significance and strength
635 of each pairwise association between retinal RGC marker and the cognitive function score. P and
636 *r*-values presented in bold type with asterisk(s) are statistically significant (<0.05). CDR, Clinical
637 Dementia Rating; MMSE, Mini-Mental State Examination.

638

639

640

641

642

643

Declarations

Acknowledgments: We thank Elijiah Maxfield for assisting with manuscript editing. We thank Prof. Carol Ann Miller, the former director of the USC-ADRC neuropathology core laboratory, for providing the neuropathological reports. We thank the late Prof. Peter Davies of The Litwin-Zucker Research Center for the Study of Alzheimer's Disease, The Feinstein Institutes for Medical Research, New York, for generously providing the PHF-1 antibodies. We thank Profs. Giovanni Meli and Antonino Cattaneo for providing antibodies against Aβ oligomers (scFvA13). The authors dedicate this manuscript to the memory of Dr. Salomon Moni Hamaoui and Lillian Jones Black, both of whom died from Alzheimer's disease.

Competing interest: The authors declare no conflict of interest relevant for this study.

Funding sources: This work has been supported by the National Institutes of Health (NIH)/the National Institute on Aging (NIA) through the following grants: R01 AG055865 and R01 AG056478 (M.K.H.), The Hertz Innovation Fund (M.K.H.), and the Gordon, Wilstein, and Saban Private Foundations (M.K.H.). M.R.D. and E.R. are supported by The Ray Charles Foundation and E.S.G. is supported by José Castillejo grants for mobility stays abroad for young doctors 2023 (CAS22/00049, Ministerio de Ciencia, Investigación y Universidades) and Complutense del Amo Grants 2023, Complutense University of Madrid.

Ethic approval and Consent to participate: This study is not considered a human subjects research, and we confirm that consent was not necessary, for the reasons described as follow: we processed and analyzed deidentified retinal tissues of deceased patients that were provided by the USC-ADRC (IRB protocol HS-042071) and NDRI (Cedars-Sinai Medical Center IRB protocol

Pro00019393). Histological studies at Cedars-Sinai Medical Center were performed under IRB protocols Pro00053412 and Pro00019393.

Author contributions: M.R.D.: performed experiments, collected, and analyzed data, created figures, drafted and edited the manuscript. E.R., A.R., B.P.G., E.S.-G.: performed experiments, collected, and analyzed data. D.-T.F.: analyzed data, created figures and illustrations, edited the manuscript. Y.K.: performed experiments, analyzed data, assisted in creating figures, wrote and edited the manuscript. N.M.: assisted with experimental design and execution, collected data. L.S., D.H. provided donor eyes and the clinical and brain pathological data. R.K.: provided the T22 antibodies that recognize tau oligomers. A.A.S., A.V.L, K.L.B.: assisted with interpretation of data and editing. M.K.-H. was responsible for study conception and design, data analysis and collection, interpretation of data, study supervision, and manuscript writing and editing. All authors have read and approved the manuscript.

Consent for publication section: Not applicable

Availability of data and material. Data generated and analyzed in this study are included in this published manuscript and the supplementary online material. Additional data can be made available by the corresponding PI upon reasonable request.

References

1 (2024) 2024 Alzheimer's disease facts and figures. Alzheimers Dement 20: 3708-3821 Doi 10.1002/alz.13809

2 Alexandrov PN, Pogue A, Bhattacharjee S, Lukiw WJ (2011) Retinal amyloid peptides and complement factor H in transgenic models of Alzheimer's disease. Neuroreport 22: 623-627 Doi 10.1097/WNR.0b013e3283497334

3 Arendt T, Bruckner MK, Morawski M, Jager C, Gertz HJ (2015) Early neurone loss in Alzheimer's disease: cortical or subcortical? Acta Neuropathol Commun 3: 10 Doi 10.1186/s40478-015-0187-1

4 Asanad S, Fantini M, Sultan W, Nassisi M, Felix CM, Wu J, Karanjia R, Ross-Cisneros FN, Sagare AP, Zlokovic BVet al (2020) Retinal nerve fiber layer thickness predicts CSF amyloid/tau before cognitive decline. PLoS One 15: e0232785 Doi 10.1371/journal.pone.0232785

5 Asanad S, Felix CM, Fantini M, Harrington MG, Sadun AA, Karanjia R (2021) Retinal ganglion cell dysfunction in preclinical Alzheimer's disease: an electrophysiologic biomarker signature. Sci Rep 11: 6344 Doi 10.1038/s41598-021-85010-1

6 Asanad S, Ross-Cisneros FN, Nassisi M, Barron E, Karanjia R, Sadun AA (2019) The Retina in Alzheimer's Disease: Histomorphometric Analysis of an Ophthalmologic Biomarker. Invest Ophthalmol Vis Sci 60: 1491-1500 Doi 10.1167/iovs.18-25966

7 Ashraf G, McGuinness M, Khan MA, Obtinalla C, Hadoux X, van Wijngaarden P (2023) Retinal imaging biomarkers of Alzheimer's disease: A systematic review and meta-analysis of studies using brain amyloid beta status for case definition. Alzheimers Dement (Amst) 15: e12421 Doi 10.1002/dad2.12421

8 Augustinack JC, Schneider A, Mandelkow EM, Hyman BT (2002) Specific tau phosphorylation sites correlate with severity of neuronal cytopathology in Alzheimer's disease. Acta Neuropathol 103: 26-35 Doi 10.1007/s004010100423

9 Baker-Nigh A, Vahedi S, Davis EG, Weintraub S, Bigio EH, Klein WL, Geula C (2015) Neuronal amyloid-beta accumulation within cholinergic basal forebrain in ageing and Alzheimer's disease. Brain 138: 1722-1737 Doi 10.1093/brain/awv024

10 Balendra SI, Normando EM, Bloom PA, Cordeiro MF (2015) Advances in retinal ganglion cell imaging. Eye (Lond) 29: 1260-1269 Doi 10.1038/eye.2015.154

11 Balusu S, De Strooper B (2024) The necroptosis cell death pathway drives neurodegeneration in Alzheimer's disease. Acta Neuropathol 147: 96 Doi 10.1007/s00401-024-02747-5

12 Besser L, Kukull W, Knopman DS, Chui H, Galasko D, Weintraub S, Jicha G, Carlsson C, Burns J, Quinn Jet al (2018) Version 3 of the National Alzheimer's Coordinating Center's Uniform Data Set. Alzheimer Dis Assoc Disord 32: 351-358 Doi 10.1097/WAD.0000000000000279

13 Bevan RJ, Hughes TR, Williams PA, Good MA, Morgan BP, Morgan JE (2020) Retinal ganglion cell degeneration correlates with hippocampal spine loss in experimental Alzheimer's disease. Acta Neuropathol Commun 8: 216 Doi 10.1186/s40478-020-01094-2

14 Blair LJ, Nordhues BA, Hill SE, Scaglione KM, O'Leary JC, 3rd, Fontaine SN, Breydo L, Zhang B, Li P, Wang Let al (2013) Accelerated neurodegeneration through chaperone-mediated oligomerization of tau. J Clin Invest 123: 4158-4169 Doi 10.1172/JCI69003

15 Blanks JC, Hinton DR, Sadun AA, Miller CA (1989) Retinal ganglion cell degeneration in Alzheimer's disease. Brain Res 501: 364-372 Doi 10.1016/0006-8993(89)90653-7

16 Blanks JC, Schmidt SY, Torigoe Y, Porrello KV, Hinton DR, Blanks RH (1996) Retinal pathology in Alzheimer's disease. II. Regional neuron loss and glial changes in GCL. Neurobiol Aging 17: 385-395 Doi 10.1016/0197-4580(96)00009-7

17 Blanks JC, Torigoe Y, Hinton DR, Blanks RH (1996) Retinal pathology in Alzheimer's disease. I. Ganglion cell loss in foveal/parafoveal retina. Neurobiol Aging 17: 377-384 Doi 10.1016/0197-4580(96)00010-3

18 Bloom GS (2014) Amyloid-beta and tau: the trigger and bullet in Alzheimer disease pathogenesis. JAMA Neurol 71: 505-508 Doi 10.1001/jamaneurol.2013.5847

19 Braak H, Alafuzoff I, Arzberger T, Kretzschmar H, Del Tredici K (2006) Staging of Alzheimer disease-associated neurofibrillary pathology using paraffin sections and immunocytochemistry. Acta Neuropathol 112: 389-404 Doi 10.1007/s00401-006-0127-z

20 Brier MR, Gordon B, Friedrichsen K, McCarthy J, Stern A, Christensen J, Owen C, Aldea P, Su Y, Hassenstab Jet al (2016) Tau and Abeta imaging, CSF measures, and cognition in Alzheimer's disease. Sci Transl Med 8: 338ra366 Doi 10.1126/scitranslmed.aaf2362

21 Caccamo A, Branca C, Piras IS, Ferreira E, Huentelman MJ, Liang WS, Readhead B, Dudley JT, Spangenberg EE, Green KNet al (2017) Necroptosis activation in Alzheimer's disease. Nat Neurosci 20: 1236-1246 Doi 10.1038/nn.4608

22 Cao KJ, Kim JH, Kroeger H, Gaffney PM, Lin JH, Sigurdson CJ, Yang J (2021) ARCAM-1 Facilitates Fluorescence Detection of Amyloid-Containing Deposits in the Retina. Transl Vis Sci Technol 10: 5 Doi 10.1167/tvst.10.7.5

23 Chen S, Zhang D, Zheng H, Cao T, Xia K, Su M, Meng Q (2023) The association between retina thinning and hippocampal atrophy in Alzheimer's disease and mild cognitive impairment: a meta-analysis and systematic review. Front Aging Neurosci 15: 1232941 Doi 10.3389/fnagi.2023.1232941

24 Chiasseu M, Alarcon-Martinez L, Belforte N, Quintero H, Dotigny F, Destroismaisons L, Vande Velde C, Panayi F, Louis C, Di Polo A (2017) Tau accumulation in the retina promotes early neuronal dysfunction and precedes brain pathology in a mouse model of Alzheimer's disease. Mol Neurodegener 12: 58 Doi 10.1186/s13024-017-0199-3

25 Coppola G, Di Renzo A, Ziccardi L, Martelli F, Fadda A, Manni G, Barboni P, Pierelli F, Sadun AA, Parisi V (2015) Optical Coherence Tomography in Alzheimer's Disease: A Meta-Analysis. PLoS One 10: e0134750 Doi 10.1371/journal.pone.0134750

26 Cordeiro MF, Hill D, Patel R, Corazza P, Maddison J, Younis S (2022) Detecting retinal cell stress and apoptosis with DARC: Progression from lab to clinic. Prog Retin Eye Res 86: 100976 Doi 10.1016/j.preteyeres.2021.100976

27 den Haan J, Morrema THJ, Verbraak FD, de Boer JF, Scheltens P, Rozemuller AJ, Bergen AAB, Bouwman FH, Hoozemans JJ (2018) Amyloid-beta and phosphorylated tau in post-mortem Alzheimer's disease retinas. Acta Neuropathol Commun 6: 147 Doi 10.1186/s40478-018-0650-x

763 28 Dong Y, Yu H, Li X, Bian K, Zheng Y, Dai M, Feng X, Sun Y, He Y, Yu Bet al (2022) Hyperphosphorylated tau mediates neuronal death by inducing necroptosis and inflammation in Alzheimer's disease. J Neuroinflammation 19: 205 Doi 10.1186/s12974-022-02567-y

766 29 Du X, Koronyo Y, Mirzaei N, Yang C, Fuchs DT, Black KL, Koronyo-Hamaoui M, Gao L (2022) Label-free hyperspectral imaging and deep-learning prediction of retinal amyloid beta-protein and phosphorylated tau. PNAS Nexus 1: pgac164 Doi 10.1093/pnasnexus/pgac164

769 30 Dumitrascu OM, Lyden PD, Torbati T, Sheyn J, Sherzai A, Sherzai D, Sherman DS, Rosenberry R, Cheng S, Johnson KOet al (2020) Sectoral segmentation of retinal amyloid imaging in subjects with cognitive decline. Alzheimers Dement (Amst) 12: e12109 Doi 10.1002/dad2.12109

772 31 Dumitrascu OM, Rosenberry R, Sherman DS, Khansari MM, Sheyn J, Torbati T, Sherzai A, Sherzai D, Johnson KO, Czeszynski ADet al (2021) Retinal Venular Tortuosity Jointly with Retinal Amyloid Burden Correlates with Verbal Memory Loss: A Pilot Study. Cells 10: Doi 10.3390/cells10112926

775 32 Elvira-Hurtado L, Lopez-Cuenca I, de Hoz R, Salas M, Sanchez-Puebla L, Ramirez-Torano F, Matamoros JA, Fernandez-Albarral JA, Rojas P, Alfonsin Set al (2023) Alzheimer's disease: a continuum with visual involvements. Front Psychol 14: 1124830 Doi 10.3389/fpsyg.2023.1124830

778 33 Erskine L, Herrera E (2014) Connecting the retina to the brain. ASN Neuro 6: Doi 10.1177/1759091414562107

780 34 Folstein MF, Folstein SE, McHugh PR (1975) "Mini-mental state". A practical method for grading the cognitive state of patients for the clinician. J Psychiatr Res 12: 189-198 Doi 10.1016/0022-3956(75)90026-6

783 35 Frontzkowski L, Ewers M, Brendel M, Biel D, Ossenkoppele R, Hager P, Steward A, Dewenter A, Romer S, Rubinski Aet al (2022) Earlier Alzheimer's disease onset is associated with tau pathology in brain hub regions and facilitated tau spreading. Nat Commun 13: 4899 Doi 10.1038/s41467-022-32592-7

787 36 Furcila D, Dominguez-Alvaro M, DeFelipe J, Alonso-Nanclares L (2019) Subregional Density of Neurons, Neurofibrillary Tangles and Amyloid Plaques in the Hippocampus of Patients With Alzheimer's Disease. Front Neuroanat 13: 99 Doi 10.3389/fnana.2019.00099

790 37 Gaire BP, Koronyo Y, Fuchs D-T, Shi H, Rentsendorj A, Danziger R, Vit J-PS, Mirzaei N, Doustar J, Sheyn Jet al (2024) Alzheimer's Disease Pathophysiology in the Retina. Progress in Retinal and Eye Research: 101273 Doi https://doi.org/10.1016/j.preteyeres.2024.101273

793 38 Gastard MC, Troncoso JC, Koliatsos VE (2003) Caspase activation in the limbic cortex of subjects with early Alzheimer's disease. Ann Neurol 54: 393-398 Doi 10.1002/ana.10680

795 39 Greenberg SM, Bacskai BJ, Hernandez-Guillamon M, Pruzin J, Sperling R, van Veluw SJ (2020) Cerebral amyloid angiopathy and Alzheimer disease - one peptide, two pathways. Nat Rev Neurol 16: 30-42 Doi 10.1038/s41582-019-0281-2

798 40 Grimaldi A, Pediconi N, Oieni F, Pizzarelli R, Rosito M, Giubettini M, Santini T, Limatola C, Ruocco G, Ragozzino Det al (2019) Neuroinflammatory Processes, A1 Astrocyte Activation and Protein Aggregation in the Retina of Alzheimer's Disease Patients, Possible Biomarkers for Early Diagnosis. Front Neurosci 13: 925 Doi 10.3389/fnins.2019.00925

802 41 Groot C, Smith R, Stomrud E, Binette AP, Leuzy A, Wuestefeld A, Wisse LEM, Palmqvist S, Mattsson-Carlgren N, Janelidze Set al (2023) Phospho-tau with subthreshold tau-PET predicts

804 increased tau accumulation rates in amyloid-positive individuals. Brain 146: 1580-1591 Doi
805 10.1093/brain/awac329

806 42 Grundke-Iqbal I, Iqbal K, Tung YC, Quinlan M, Wisniewski HM, Binder LI (1986) Abnormal
807 phosphorylation of the microtubule-associated protein tau (tau) in Alzheimer cytoskeletal
808 pathology. Proc Natl Acad Sci U S A 83: 4913-4917 Doi 10.1073/pnas.83.13.4913

809 43 Hadoux X, Hui F, Lim JKH, Masters CL, Pebay A, Chevalier S, Ha J, Loi S, Fowler CJ, Rowe Cet al
810 (2019) Non-invasive in vivo hyperspectral imaging of the retina for potential biomarker use in
811 Alzheimer's disease. Nat Commun 10: 4227 Doi 10.1038/s41467-019-12242-1

812 44 Hammer DX, Agrawal A, Villanueva R, Saeedi O, Liu Z (2020) Label-free adaptive optics imaging of
813 human retinal macrophage distribution and dynamics. Proc Natl Acad Sci U S A 117: 30661-30669
814 Doi 10.1073/pnas.2010943117

815 45 Hart de Ruyter FJ, Evers M, Morrema THJ, Dijkstra AA, den Haan J, Twisk JWR, de Boer JF, Scheltens
816 P, Bouwman FH, Verbraak FDet al (2024) Neuropathological hallmarks in the post-mortem retina
817 of neurodegenerative diseases. Acta Neuropathol 148: 24 Doi 10.1007/s00401-024-02769-z

818 46 Hart de Ruyter FJ, Morrema THJ, den Haan J, Netherlands Brain B, Twisk JWR, de Boer JF, Scheltens
819 P, Boon BDC, Thal DR, Rozemuller AJet al (2022) Phosphorylated tau in the retina correlates with
820 tau pathology in the brain in Alzheimer's disease and primary tauopathies. Acta Neuropathol: Doi
821 10.1007/s00401-022-02525-1

822 47 Hart NJ, Koronyo Y, Black KL, Koronyo-Hamaoui M (2016) Ocular indicators of Alzheimer's:
823 exploring disease in the retina. Acta Neuropathol 132: 767-787 Doi 10.1007/s00401-016-1613-6

824 48 Hinton DR, Sadun AA, Blanks JC, Miller CA (1986) Optic-nerve degeneration in Alzheimer's disease.
825 N Engl J Med 315: 485-487 Doi 10.1056/NEJM198608213150804

826 49 Hyman BT, Phelps CH, Beach TG, Bigio EH, Cairns NJ, Carrillo MC, Dickson DW, Duyckaerts C,
827 Frosch MP, Masliah Eet al (2012) National Institute on Aging-Alzheimer's Association guidelines
828 for the neuropathologic assessment of Alzheimer's disease. Alzheimers Dement 8: 1-13 Doi
829 10.1016/j.jalz.2011.10.007

830 50 Iqbal K, Wisniewski HM, Shelanski ML, Brostoff S, Liwnicz BH, Terry RD (1974) Protein changes in
831 senile dementia. Brain Res 77: 337-343 Doi 10.1016/0006-8993(74)90798-7

832 51 Jack CR, Jr., Bennett DA, Blennow K, Carrillo MC, Dunn B, Haeberlein SB, Holtzman DM, Jagust W,
833 Jessen F, Karlawish Jet al (2018) NIA-AA Research Framework: Toward a biological definition of
834 Alzheimer's disease. Alzheimers Dement 14: 535-562 Doi 10.1016/j.jalz.2018.02.018

835 52 Kadar A, Wittmann G, Liposits Z, Fekete C (2009) Improved method for combination of
836 immunocytochemistry and Nissl staining. J Neurosci Methods 184: 115-118 Doi
837 10.1016/j.jneumeth.2009.07.010

838 53 Katz B, Rimmer S, Iragui V, Katzman R (1989) Abnormal pattern electroretinogram in Alzheimer's
839 disease: evidence for retinal ganglion cell degeneration? Ann Neurol 26: 221-225 Doi
840 10.1002/ana.410260207

841 54 Kfoury N, Holmes BB, Jiang H, Holtzman DM, Diamond MI (2012) Trans-cellular propagation of
842 Tau aggregation by fibrillar species. J Biol Chem 287: 19440-19451 Doi 10.1074/jbc.M112.346072

843 55 Kim US, Mahroo OA, Mollon JD, Yu-Wai-Man P (2021) Retinal Ganglion Cells-Diversity of Cell Types
844 and Clinical Relevance. Front Neurol 12: 661938 Doi 10.3389/fneur.2021.661938

845 56 Kirbas S, Turkyilmaz K, Anlar O, Tufekci A, Durmus M (2013) Retinal nerve fiber layer thickness in
846 patients with Alzheimer disease. J Neuroophthalmol 33: 58-61 Doi
847 10.1097/WNO.0b013e318267fd5f

848 57 Kivela T (1998) Parvalbumin, a horizontal cell-associated calcium-binding protein in
849 retinoblastoma eyes. Invest Ophthalmol Vis Sci 39: 1044-1048

850 58 Kopeikina KJ, Hyman BT, Spires-Jones TL (2012) Soluble forms of tau are toxic in Alzheimer's
851 disease. Transl Neurosci 3: 223-233 Doi 10.2478/s13380-012-0032-y

852 59 Koper MJ, Van Schoor E, Ospitalieri S, Vandenberghe R, Vandenbulcke M, von Arnim CAF,
853 Tousseyn T, Balusu S, De Strooper B, Thal DR (2020) Necrosome complex detected in
854 granulovacuolar degeneration is associated with neuronal loss in Alzheimer's disease. Acta
855 Neuropathol 139: 463-484 Doi 10.1007/s00401-019-02103-y

856 60 Koronyo Y, Biggs D, Barron E, Boyer DS, Pearlman JA, Au WJ, Kile SJ, Blanco A, Fuchs DT, Ashfaq
857 Aet al (2017) Retinal amyloid pathology and proof-of-concept imaging trial in Alzheimer's disease.
858 JCI Insight 2: Doi 10.1172/jci.insight.93621

859 61 Koronyo Y, Rentsendorj A, Mirzaei N, Regis GC, Sheyn J, Shi H, Barron E, Cook-Wiens G, Rodriguez
860 AR, Medeiros Ret al (2023) Retinal pathological features and proteome signatures of Alzheimer's
861 disease. Acta Neuropathol 145: 409-438 Doi 10.1007/s00401-023-02548-2

862 62 Koronyo-Hamaoui M, Koronyo Y, Ljubimov AV, Miller CA, Ko MK, Black KL, Schwartz M, Farkas DL
863 (2011) Identification of amyloid plaques in retinas from Alzheimer's patients and noninvasive in
864 vivo optical imaging of retinal plaques in a mouse model. Neuroimage 54 Suppl 1: S204-217 Doi
865 10.1016/j.neuroimage.2010.06.020

866 63 Kwong JM, Caprioli J, Piri N (2010) RNA binding protein with multiple splicing: a new marker for
867 retinal ganglion cells. Invest Ophthalmol Vis Sci 51: 1052-1058 Doi 10.1167/iovs.09-4098

868 64 Kyalu Ngoie Zola N, Balty C, Pyr Dit Ruys S, Vanparys AAT, Huyghe NDG, Herinckx G, Johanns M,
869 Boyer E, Kienlen-Campard P, Rider MHet al (2023) Specific post-translational modifications of
870 soluble tau protein distinguishes Alzheimer's disease and primary tauopathies. Nat Commun 14:
871 3706 Doi 10.1038/s41467-023-39328-1

872 65 La Joie R, Visani AV, Baker SL, Brown JA, Bourakova V, Cha J, Chaudhary K, Edwards L, Iaccarino L,
873 Janabi Met al (2020) Prospective longitudinal atrophy in Alzheimer's disease correlates with the
874 intensity and topography of baseline tau-PET. Sci Transl Med 12: Doi
875 10.1126/scitranslmed.aau5732

876 66 La Morgia C, Di Vito L, Carelli V, Carbonelli M (2017) Patterns of Retinal Ganglion Cell Damage in
877 Neurodegenerative Disorders: Parvocellular vs Magnocellular Degeneration in Optical Coherence
878 Tomography Studies. Front Neurol 8: 710 Doi 10.3389/fneur.2017.00710

879 67 La Morgia C, Ross-Cisneros FN, Koronyo Y, Hannibal J, Gallassi R, Cantalupo G, Sambati L, Pan BX,
880 Tozer KR, Barboni Pet al (2016) Melanopsin retinal ganglion cell loss in Alzheimer disease. Ann
881 Neurol 79: 90-109 Doi 10.1002/ana.24548

882 68 Lambert MP, Barlow AK, Chromy BA, Edwards C, Freed R, Liosatos M, Morgan TE, Rozovsky I,
883 Trommer B, Viola KLet al (1998) Diffusible, nonfibrillar ligands derived from Abeta1-42 are potent
884 central nervous system neurotoxins. Proc Natl Acad Sci U S A 95: 6448-6453 Doi
885 10.1073/pnas.95.11.6448

886 69 Laycock R, Crewther SG, Crewther DP (2007) A role for the 'magnocellular advantage' in visual
887 impairments in neurodevelopmental and psychiatric disorders. Neurosci Biobehav Rev 31: 363-
888 376 Doi 10.1016/j.neubiorev.2006.10.003

889 70 Lee S, Jiang K, McIlmoyle B, To E, Xu QA, Hirsch-Reinshagen V, Mackenzie IR, Hsiung GR, Eadie BD,
890 Sarunic MVet al (2020) Amyloid Beta Immunoreactivity in the Retinal Ganglion Cell Layer of the
891 Alzheimer's Eye. Front Neurosci 14: 758 Doi 10.3389/fnins.2020.00758

892 71 Lemmens S, Van Craenendonck T, Van Eijgen J, De Groef L, Bruffaerts R, de Jesus DA, Charle W,
893 Jayapala M, Sunaric-Megevand G, Standaert Aet al (2020) Combination of snapshot hyperspectral
894 retinal imaging and optical coherence tomography to identify Alzheimer's disease patients.
895 Alzheimers Res Ther 12: 144 Doi 10.1186/s13195-020-00715-1

896 72 Lopez-Cuenca I, Nebreda A, Garcia-Colomo A, Salobrar-Garcia E, de Frutos-Lucas J, Bruna R,
897 Ramirez AI, Ramirez-Torano F, Salazar JJ, Barabash Aet al (2023) Early visual alterations in
898 individuals at-risk of Alzheimer's disease: a multidisciplinary approach. Alzheimers Res Ther 15:
899 19 Doi 10.1186/s13195-023-01166-0

900 73 Lopez-de-Eguileta A, Lopez-Garcia S, Lage C, Pozueta A, Garcia-Martinez M, Kazimierczak M, Bravo
901 M, Irure J, Lopez-Hoyos M, Munoz-Cacho Pet al (2022) The retinal ganglion cell layer reflects
902 neurodegenerative changes in cognitively unimpaired individuals. Alzheimers Res Ther 14: 57 Doi
903 10.1186/s13195-022-00998-6

904 74 Lu Y, Li Z, Zhang X, Ming B, Jia J, Wang R, Ma D (2010) Retinal nerve fiber layer structure
905 abnormalities in early Alzheimer's disease: evidence in optical coherence tomography. Neurosci
906 Lett 480: 69-72 Doi 10.1016/j.neulet.2010.06.006

907 75 Marziani E, Pomati S, Ramolfo P, Cigada M, Giani A, Mariani C, Staurenghi G (2013) Evaluation of
908 retinal nerve fiber layer and ganglion cell layer thickness in Alzheimer's disease using spectral-
909 domain optical coherence tomography. Invest Ophthalmol Vis Sci 54: 5953-5958 Doi
910 10.1167/iovs.13-12046

911 76 Miller DT, Kurokawa K (2020) Cellular-Scale Imaging of Transparent Retinal Structures and
912 Processes Using Adaptive Optics Optical Coherence Tomography. Annu Rev Vis Sci 6: 115-148 Doi
913 10.1146/annurev-vision-030320-041255

914 77 Mirra SS, Heyman A, McKeel D, Sumi SM, Crain BJ, Brownlee LM, Vogel FS, Hughes JP, van Belle
915 G, Berg L (1991) The Consortium to Establish a Registry for Alzheimer's Disease (CERAD). Part II.
916 Standardization of the neuropathologic assessment of Alzheimer's disease. Neurology 41: 479-
917 486 Doi 10.1212/wnl.41.4.479

918 78 Mirzaei N, Shi H, Oviatt M, Doustar J, Rentsendorj A, Fuchs DT, Sheyn J, Black KL, Koronyo Y,
919 Koronyo-Hamaoui M (2020) Alzheimer's Retinopathy: Seeing Disease in the Eyes. Front Neurosci
920 14: 921 Doi 10.3389/fnins.2020.00921

921 79 Moloney CM, Lowe VJ, Murray ME (2021) Visualization of neurofibrillary tangle maturity in
922 Alzheimer's disease: A clinicopathologic perspective for biomarker research. Alzheimers Dement
923 17: 1554-1574 Doi 10.1002/alz.12321

924 80 Montine TJ, Phelps CH, Beach TG, Bigio EH, Cairns NJ, Dickson DW, Duyckaerts C, Frosch MP,
925 Masliah E, Mirra SSet al (2012) National Institute on Aging-Alzheimer's Association guidelines for
926 the neuropathologic assessment of Alzheimer's disease: a practical approach. Acta Neuropathol
927 123: 1-11 Doi 10.1007/s00401-011-0910-3

928 81 More SS, Beach JM, McClelland C, Mokhtarzadeh A, Vince R (2019) In Vivo Assessment of Retinal
929 Biomarkers by Hyperspectral Imaging: Early Detection of Alzheimer's Disease. ACS Chem Neurosci
930 10: 4492-4501 Doi 10.1021/acschemneuro.9b00331

931 82 Morris JC (1993) The Clinical Dementia Rating (CDR): current version and scoring rules. Neurology
932 43: 2412-2414 Doi 10.1212/wnl.43.11.2412-a

933 83 Mucke L, Selkoe DJ (2012) Neurotoxicity of amyloid beta-protein: synaptic and network
934 dysfunction. Cold Spring Harb Perspect Med 2: a006338 Doi 10.1101/cshperspect.a006338

935 84 Nadal-Nicolás FM, Galindo-Romero C, Lucas-Ruiz F, Marsh-Amstrong N, Li W, Vidal-Sanz M,
936 Agudo-Barriuso M (2023) Pan-retinal ganglion cell markers in mice, rats, and rhesus macaques.
937 Zool Res 44: 226-248 Doi 10.24272/j.issn.2095-8137.2022.308

938 85 Ngolab J, Donohue M, Belsha A, Salazar J, Cohen P, Jaiswal S, Tan V, Gessert D, Korouri S, Aggarwal
939 NTet al (2021) Feasibility study for detection of retinal amyloid in clinical trials: The Anti-Amyloid
940 Treatment in Asymptomatic Alzheimer's Disease (A4) trial. Alzheimers Dement (Amst) 13: e12199
941 Doi 10.1002/dad2.12199

942 86 Nunez-Diaz C, Andersson E, Schultz N, Poceviciute D, Hansson O, Netherlands Brain B, Nilsson KPR,
943 Wennstrom M (2024) The fluorescent ligand bTVBT2 reveals increased p-tau uptake by retinal
944 microglia in Alzheimer's disease patients and App(NL-F/NL-F) mice. Alzheimers Res Ther 16: 4 Doi
945 10.1186/s13195-023-01375-7

946 87 O'Bryant SE, Humphreys JD, Smith GE, Ivnik RJ, Graff-Radford NR, Petersen RC, Lucas JA (2008)
947 Detecting dementia with the mini-mental state examination in highly educated individuals. Arch
948 Neurol 65: 963-967 Doi 10.1001/archneur.65.7.963

949 88 Oku H, Kida T, Horie T, Taki K, Mimura M, Kojima S, Ikeda T (2019) Tau Is Involved in Death of
950 Retinal Ganglion Cells of Rats From Optic Nerve Crush. Invest Ophthalmol Vis Sci 60: 2380-2387
951 Doi 10.1167/iovs.19-26683

952 89 Pasparakis M, Vandenabeele P (2015) Necroptosis and its role in inflammation. Nature 517: 311-
953 320 Doi 10.1038/nature14191

954 90 Peeraer E, Bottelbergs A, Van Kolen K, Stancu IC, Vasconcelos B, Mahieu M, Duytschaever H, Ver
955 Donck L, Torremans A, Sluydts Eet al (2015) Intracerebral injection of preformed synthetic tau
956 fibrils initiates widespread tauopathy and neuronal loss in the brains of tau transgenic mice.
957 Neurobiol Dis 73: 83-95 Doi 10.1016/j.nbd.2014.08.032

958 91 Pereiro X, Ruzafa N, Urcola JH, Sharma SC, Vecino E (2020) Differential Distribution of RBPMS in
959 Pig, Rat, and Human Retina after Damage. Int J Mol Sci 21: Doi 10.3390/ijms21239330

960 92 Piri N, Kwong JM, Song M, Caprioli J (2006) Expression of hermes gene is restricted to the ganglion
961 cells in the retina. Neurosci Lett 405: 40-45 Doi 10.1016/j.neulet.2006.06.049

962 93 Purves D. AGJ, Fitzpatrick D., Katz L. C. , LaMantia A.-S., McNamara J. O., William S. M. (2001)
963 Neuroscience, 2nd edition. Sunderland (MA): Sinauer Associates, City

964 94 Qiu Y, Jin T, Mason E, Campbell MCW (2020) Predicting Thioflavin Fluorescence of Retinal Amyloid
965 Deposits Associated With Alzheimer's Disease from Their Polarimetric Properties. Transl Vis Sci
966 Technol 9: 47 Doi 10.1167/tvst.9.2.47

967 95 Rawat P, Sehar U, Bisht J, Selman A, Culberson J, Reddy PH (2022) Phosphorylated Tau in
968 Alzheimer's Disease and Other Tauopathies. Int J Mol Sci 23: Doi 10.3390/ijms232112841

96 Regalado-Reyes M, Furcila D, Hernandez F, Avila J, DeFelipe J, Leon-Espinosa G (2019) Phospho-Tau Changes in the Human CA1 During Alzheimer's Disease Progression. J Alzheimers Dis 69: 277-288 Doi 10.3233/JAD-181263

97 Risacher SL, WuDunn D, Tallman EF, West JD, Gao S, Farlow MR, Brosch JR, Apostolova LG, Saykin AJ (2020) Visual contrast sensitivity is associated with the presence of cerebral amyloid and tau deposition. Brain Commun 2: fcaa019 Doi 10.1093/braincomms/fcaa019

98 Rodriguez AR, de Sevilla Müller LP, Brecha NC (2014) The RNA binding protein RBPMS is a selective marker of ganglion cells in the mammalian retina. J Comp Neurol 522: 1411-1443 Doi 10.1002/cne.23521

99 Rossetti HC, Munro Cullum C, Hynan LS, Lacritz LH (2010) The CERAD Neuropsychologic Battery Total Score and the progression of Alzheimer disease. Alzheimer Dis Assoc Disord 24: 138-142 Doi 10.1097/WAD.0b013e3181b76415

100 Sadun AA, Borchert M, DeVita E, Hinton DR, Bassi CJ (1987) Assessment of visual impairment in patients with Alzheimer's disease. Am J Ophthalmol 104: 113-120 Doi 10.1016/0002-9394(87)90001-8

101 Salobrar-Garcia E, de Hoz R, Ramirez AI, Lopez-Cuenca I, Rojas P, Vazirani R, Amarante C, Yubero R, Gil P, Pinazo-Duran MDet al (2019) Changes in visual function and retinal structure in the progression of Alzheimer's disease. PLoS One 14: e0220535 Doi 10.1371/journal.pone.0220535

102 Sanes JR, Masland RH (2015) The types of retinal ganglion cells: current status and implications for neuronal classification. Annu Rev Neurosci 38: 221-246 Doi 10.1146/annurev-neuro-071714-034120

103 Schön C, Hoffmann NA, Ochs SM, Burgold S, Filser S, Steinbach S, Seeliger MW, Arzberger T, Goedert M, Kretzschmar HAet al (2012) Long-term in vivo imaging of fibrillar tau in the retina of P301S transgenic mice. PLoS One 7: e53547 Doi 10.1371/journal.pone.0053547

104 Schultz N, Byman E, Wennström M (2020) Levels of Retinal Amyloid-β Correlate with Levels of Retinal IAPP and Hippocampal Amyloid-β in Neuropathologically Evaluated Individuals. J Alzheimers Dis 73: 1201-1209 Doi 10.3233/jad-190868

105 Serrano-Pozo A, Frosch MP, Masliah E, Hyman BT (2011) Neuropathological alterations in Alzheimer disease. Cold Spring Harb Perspect Med 1: a006189 Doi 10.1101/cshperspect.a006189

106 Shi H, Koronyo Y, Fuchs DT, Sheyn J, Jallow O, Mandalia K, Graham SL, Gupta VK, Mirzaei M, Kramerov AAet al (2023) Retinal arterial Abeta(40) deposition is linked with tight junction loss and cerebral amyloid angiopathy in MCI and AD patients. Alzheimers Dement: Doi 10.1002/alz.13086

107 Shi H, Koronyo Y, Rentsendorj A, Regis GC, Sheyn J, Fuchs DT, Kramerov AA, Ljubimov AV, Dumitrascu OM, Rodriguez ARet al (2020) Identification of early pericyte loss and vascular amyloidosis in Alzheimer's disease retina. Acta Neuropathol 139: 813-836 Doi 10.1007/s00401-020-02134-w

108 Shi H, Mirzaei N, Koronyo Y, Davis MR, Robinson E, Braun GM, Jallow O, Rentsendorj A, Ramanujan VK, Fert-Bober Jet al (2024) Identification of retinal oligomeric, citrullinated, and other tau isoforms in early and advanced AD and relations to disease status. Acta Neuropathol 148: 3 Doi 10.1007/s00401-024-02760-8

109 Snyder PJ, Alber J, Alt C, Bain LJ, Bouma BE, Bouwman FH, DeBuc DC, Campbell MCW, Carrillo MC, Chew EYet al (2021) Retinal imaging in Alzheimer's and neurodegenerative diseases. Alzheimers Dement 17: 103-111 Doi 10.1002/alz.12179

110 Sperling RA, Aisen PS, Beckett LA, Bennett DA, Craft S, Fagan AM, Iwatsubo T, Jack CR, Jr., Kaye J, Montine TJet al (2011) Toward defining the preclinical stages of Alzheimer's disease: recommendations from the National Institute on Aging-Alzheimer's Association workgroups on diagnostic guidelines for Alzheimer's disease. Alzheimers Dement 7: 280-292 Doi 10.1016/j.jalz.2011.03.003

111 Sperling RA, Donohue MC, Raman R, Sun CK, Yaari R, Holdridge K, Siemers E, Johnson KA, Aisen PS, Team AS (2020) Association of Factors With Elevated Amyloid Burden in Clinically Normal Older Individuals. JAMA Neurol 77: 735-745 Doi 10.1001/jamaneurol.2020.0387

112 Su JH, Zhao M, Anderson AJ, Srinivasan A, Cotman CW (2001) Activated caspase-3 expression in Alzheimer's and aged control brain: correlation with Alzheimer pathology. Brain Res 898: 350-357 Doi 10.1016/s0006-8993(01)02018-2

113 Tadokoro K, Yamashita T, Kimura S, Nomura E, Ohta Y, Omote Y, Takemoto M, Hishikawa N, Morihara R, Morizane Yet al (2021) Retinal Amyloid Imaging for Screening Alzheimer's Disease. J Alzheimers Dis 83: 927-934 Doi 10.3233/JAD-210327

114 Tai HC, Serrano-Pozo A, Hashimoto T, Frosch MP, Spires-Jones TL, Hyman BT (2012) The synaptic accumulation of hyperphosphorylated tau oligomers in Alzheimer disease is associated with dysfunction of the ubiquitin-proteasome system. Am J Pathol 181: 1426-1435 Doi 10.1016/j.ajpath.2012.06.033

115 Thal DR, Rüb U, Orantes M, Braak H (2002) Phases of A beta-deposition in the human brain and its relevance for the development of AD. Neurology 58: 1791-1800 Doi 10.1212/wnl.58.12.1791

116 Theofilas P, Ehrenberg AJ, Nguy A, Thackrey JM, Dunlop S, Mejia MB, Alho AT, Paraizo Leite RE, Rodriguez RD, Suemoto CKet al (2018) Probing the correlation of neuronal loss, neurofibrillary tangles, and cell death markers across the Alzheimer's disease Braak stages: a quantitative study in humans. Neurobiol Aging 61: 1-12 Doi 10.1016/j.neurobiolaging.2017.09.007

117 Thomsen ND, Koerber JT, Wells JA (2013) Structural snapshots reveal distinct mechanisms of procaspase-3 and -7 activation. Proc Natl Acad Sci U S A 110: 8477-8482 Doi 10.1073/pnas.1306759110

118 Trick GL, Barris MC, Bickler-Bluth M (1989) Abnormal pattern electroretinograms in patients with senile dementia of the Alzheimer type. Ann Neurol 26: 226-231 Doi 10.1002/ana.410260208

119 Uchihara T (2007) Silver diagnosis in neuropathology: principles, practice and revised interpretation. Acta Neuropathol 113: 483-499 Doi 10.1007/s00401-007-0200-2

120 van der Gaag BL, Deshayes NAC, Breve JJP, Bol J, Jonker AJ, Hoozemans JJM, Courade JP, van de Berg WDJ (2024) Distinct tau and alpha-synuclein molecular signatures in Alzheimer's disease with and without Lewy bodies and Parkinson's disease with dementia. Acta Neuropathol 147: 14 Doi 10.1007/s00401-023-02657-y

121 VanderWall KB, Lu B, Alfaro JS, Allsop AR, Carr AS, Wang S, Meyer JS (2020) Differential susceptibility of retinal ganglion cell subtypes in acute and chronic models of injury and disease. Sci Rep 10: 17359 Doi 10.1038/s41598-020-71460-6

122 Walkiewicz G, Ronisz A, Van Ginderdeuren R, Lemmens S, Bouwman FH, Hoozemans JJM, Morrema THJ, Rozemuller AJ, Hart de Ruyter FJ, De Groef Let al (2023) Primary retinal tauopathy: A tauopathy with a distinct molecular pattern. Alzheimers Dement: Doi 10.1002/alz.13424

123 Xu QA, Boerkoel P, Hirsch-Reinshagen V, Mackenzie IR, Hsiung GR, Charm G, To EF, Liu AQ, Schwab K, Jiang Ket al (2022) Muller cell degeneration and microglial dysfunction in the Alzheimer's retina. Acta Neuropathol Commun 10: 145 Doi 10.1186/s40478-022-01448-y

124 Yarns BC, Holiday KA, Carlson DM, Cosgrove CK, Melrose RJ (2022) Pathophysiology of Alzheimer's Disease. Psychiatr Clin North Am 45: 663-676 Doi 10.1016/j.psc.2022.07.003

125 Zhang R, Song Y, Su X (2023) Necroptosis and Alzheimer's Disease: Pathogenic Mechanisms and Therapeutic Opportunities. J Alzheimers Dis 94: S367-S386 Doi 10.3233/JAD-220809

126 Zhang Y, Chen H, Li R, Sterling K, Song W (2023) Amyloid beta-based therapy for Alzheimer's disease: challenges, successes and future. Signal Transduct Target Ther 8: 248 Doi 10.1038/s41392-023-01484-7

127 Zhao B, Li Y, Fan Z, Wu Z, Shu J, Yang X, Yang Y, Wang X, Li B, Wang Xet al (2024) Eye-brain connections revealed by multimodal retinal and brain imaging genetics. Nat Commun 15: 6064 Doi 10.1038/s41467-024-50309-w

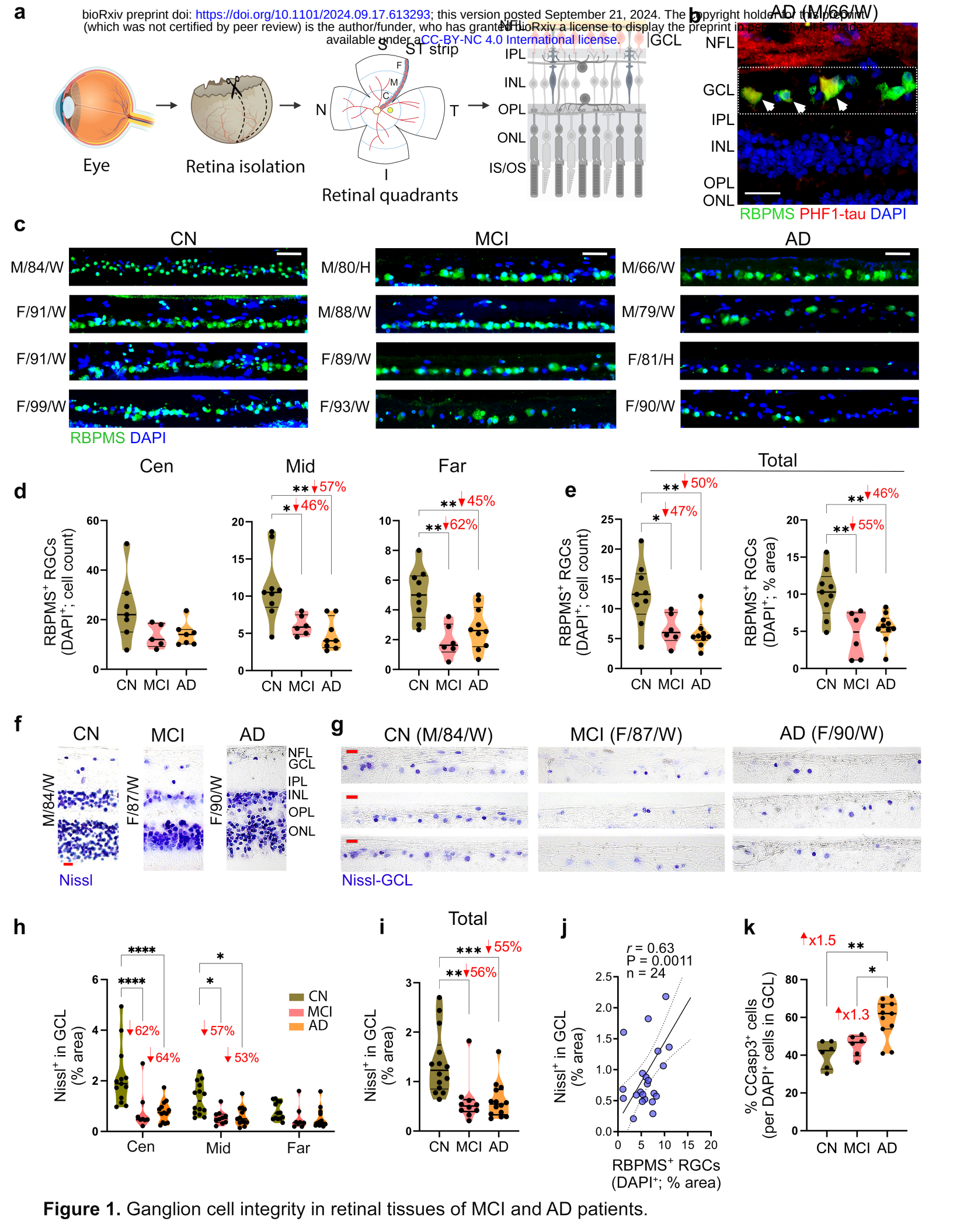

Figure 1. Ganglion cell integrity in retinal tissues of MCI and AD patients.

Figure Legends:

Figure 1. Ganglion cell integrity in retinal tissues of MCI and AD patients.

a Illustration of the histological process, including retinal isolation, cross-section preparation, and analysis of the superior temporal (ST) strip, extending from the optic disc to the ora serrata and anatomically predefined into central (Cen), middle (Mid) and far-peripheral (Far) subregions. The retinal ganglion cell layer (GCL) was analyzed in this study. **b** Microscopic image of a retinal cross-section from an AD patient, immunolabeled with retinal ganglion cell (RGC)-specific marker, ribonucleic acid binding protein with multiple splicing (RBPMS; green), and paired-helical filament of tau (PHF1-tau; red), along with nuclei labelling with DAPI (blue). Scale bar: 25 µm. **c** Representative microscopic images of $RBPMS^+$ RGCs within the GCL, labeled with RBPMS (green) and DAPI (blue), in retinal cross-sections from patients with mild cognitive impairment (MCI due to AD, n=4) and Alzheimer's disease (AD) dementia (n=4), and cognitively normal individuals (CN, n=4). Scale bar: 50 µm. **d, e** Violin graphs display the quantitative immunohistochemistry analyses of $RBPMS^+DAPI^+$ RGCs by **d** cell count in Cen, Mid- and Far-peripheral subregions, and **e** cell count (left) and percent area (right) in the total ST region (n=25 subjects; n=9 CN, n=6 MCI, n=10 AD). **f, g** Representative microscopic images of retinal cross-sections from CN, MCI, and AD donors labeled with Nissl stain (purple) in **f** all analyzed retinal layers (ONL to NFL) and **g** GCL separately. Scale bars: 20 µm. **g, h** Quantitative analyses of $Nissl^+$ percent area in GCL in **g** the Cen, Mid, and Far-peripheral subregions (n=33-37) and **h** the total ST region (n=38 subjects; n=14 CN, n=10 MCI, n=14 AD). **i** Pearson's correlation coefficient (*r*) analysis between $RBPMS^+$ RGCs percent area and $Nissl^+$ cells (in GCL) percent area. **j** Quantitative analysis of the percent area of early apoptotic cell marker, cleaved caspase-3 $(CCasp3)^+$ in GCL, normalized to nuclei count (n=23 subjects; n=6 CN, n=6 MCI, n=11 AD). Individual data points and median, lower and upper quartiles are shown in violin plots. *P < 0.05, **P < 0.01, ***P < 0.001, ****P < 0.0001, by one-way or two-way ANOVA followed by Tukey's post-hoc multiple comparison test. Percent decreases and fold changes are shown in red. F, female; M, male; Age (in years); Ethnicity: W, White and H, Hispanic; NFL, Nerve fiber layer; IPL, Inner Plexiform Layer; INL, Inner Nuclear Layer; OPL, Outer Plexiform Layer; ONL, Outer Nuclear Layer; IS/OS, inner segment and outer segment. Illustrations created with Biorender.com.

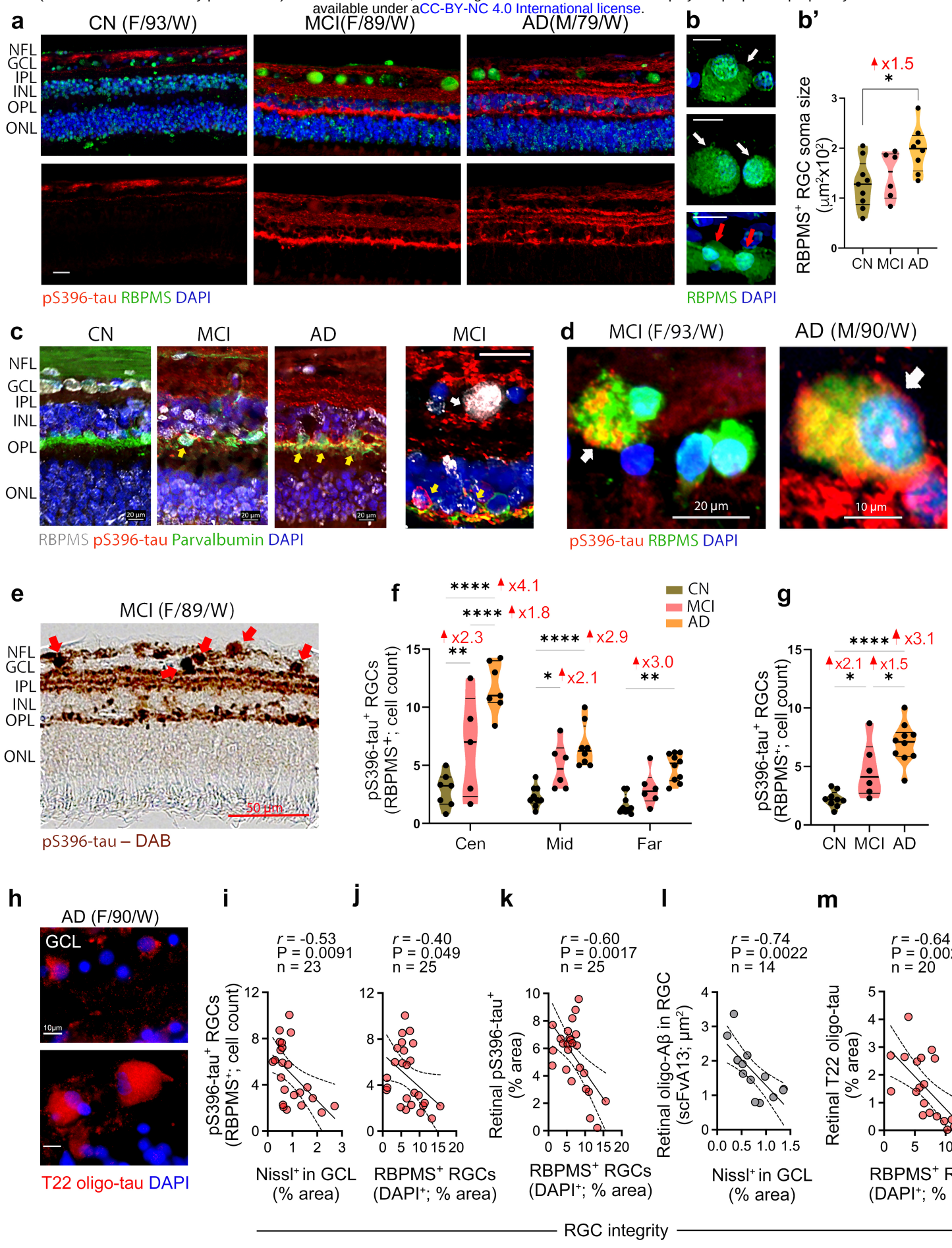

Figure 2. Pretangle tau pathology in RGCs of MCI and AD patients.

Figure 2. Pretangle tau pathology in RGCs of MCI and AD patients.

a Representative microscopic images of retinal cross-sections immunofluorescently stained for hyperphosphorylated (p)tau at S396 epitope (pS396-tau, red), RGC-specific marker, RBPMS (green) and nuclei (DAPI, blue) in retinal cross-sections from patients with mild cognitive impairment (MCI due to AD) and Alzheimer's disease (AD) dementia, and cognitively normal individuals (CN). **a, b** Retinas from MCI and AD patients exhibit increases in pS396-tau isoforms and the RGCs exhibit reduced numbers, a hypertrophic cytoplasm (cell soma swelling), and abnormal morphology, including granulovacuolar vesicles degeneration (GVD)-like bodies and nucleus displacement (white arrows indicate enlarged and granulomatous soma area and red arrows point to nuclear displacement). Scale bars: 20µm. **b'** Quantitative analysis of $RBPMS^+$ RGC soma cell size in patients with MCI (n=6) and AD (n=8), and in CN controls (n=9). **c** Representative immunofluorescent images of retinal cross- section labelled for RBPMS RGCs (white), pS396-tau (red), amacrine and RGCs marker - parvalbumin (green), and nuclei (DAPI, blue) in CN, MCI and AD subjects. Colocalization of pS396-tau in $parvalbumin^+$ amacrine cells (yellow arrows) and $RBPMS^+$ RGCs (white arrows) are shown. Scale bars: 20µm. **d** High-magnification microscopic images depicting pS396-tau accumulation (red) in swollen $RBPMS^+$ RGCs (green) with hypertrophic soma (white arrows). Scale bar sizes are indicated on images. **e** Representative microscopic image of peroxidase-based staining for pS396-tau isoforms (brown) within retinal layers, and specifically, in RGCs of a MCI patient. Scale bar: 50 µm. **f, g** Cell count of pS396-tau^+ RGCs in retinal **f** Cen, Mid- and Far-peripheral subregions (n=19-25) and **g** total ST region (n=9 CN, n=6 MCI, n=10 AD). **h** Representative images of $T22^+$ oligo-tau in the GCL of an AD patient. Scale bars: 10 µm. **i-m** Pearson's correlation coefficient (*r*) analyses between: **i** % area of $Nissl^+$ in GCL or **j** $RBPMS^+$ RGCs % area and pS396-tau^+ RGC count, **k** $RBPMS^+$ RGC % area and retinal pS396-tau^+ % area, **l** % area of $Nissl^+$ in GCL and retinal scFvA13$^+$Aβ (oligo-Aβ) in RGCs, and **m** $RBPMS^+$ RGC % area and retinal $T22^+$ tau oligomers (oligo-tau). Individual data points and median, lower and upper quartiles are shown in violin plots. *P < 0.05, **P < 0.01, ****P < 0.0001, by one-way or two-way ANOVA followed by Tukey's post-hoc multiple comparison test. Fold changes are shown in red. F, female; M, male; Age (in years); Ethnicity: W, White; NFL, Nerve fiber layer, GCL, ganglion cell layer; IPL, Inner Plexiform Layer; INL, Inner Nuclear Layer, OPL, Outer Plexiform Layer; ONL, Outer Nuclear Layer; RGC, Retinal ganglion cells.

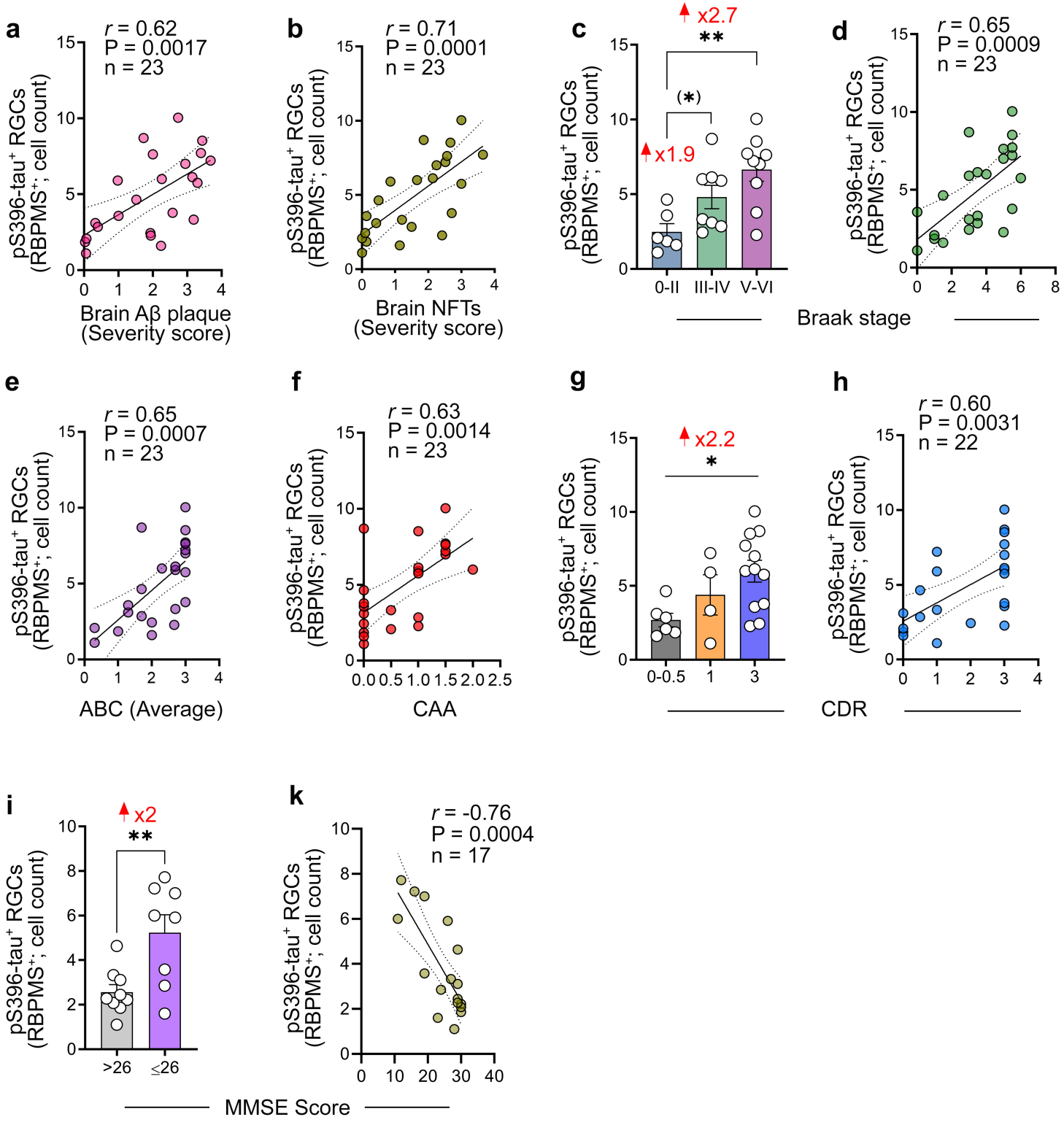

Figure 3. Interactions between retinal pS396-tau in RGCs, brain pathology, and cognitive status.

Figure 3. Interactions between retinal pS396-tau in RGCs, brain pathology, and cognitive status.

a, b Pearson's correlation coefficient (*r*) analyses between pS396-tau$^+$ RGC count and **a** brain amyloid β -protein (Aβ) plaque severity scores, or **b** brain neurofibrillary tangles (NFTs) severity scores. **c** Quantitative analysis of pS396-tau$^+$ RGC count stratified by Braak stage classification (n=23) and **d** Pearson's *r* correlations of pS396-tau$^+$ RGC count with the Braak stage. **e, f** Pearson's correlations between pS396-tau$^+$ RGC count and **e** average ABC scores and **f** cerebral amyloid angiopathy (CAA) grade. **g** Quantitative analysis of pS396-tau$^+$ RGC count stratified by clinical dementia rating (CDR) scores (n=22) and **h** Pearson's *r* correlations of pS396-tau$^+$ RGC count with the CDR scores. **i** Quantitative analysis of pS396-tau$^+$ RGC count stratified by mini-mental state examination score (MMSE) scores (n=17) and **k** Pearson's *r* correlations of pS396-tau$^+$ RGC count with the MMSE scores. Bar graphs are showing individual data points and mean ± SEM. *P < 0.05, **P < 0.01, by one-way ANOVA followed by Tukey's post-hoc multiple comparison test. Two group comparison is determined by two-tail Student t-test. ABC scores comprise of mean grades for: (A) Aβ plaque score modified from Thal, (B) NFT stage modified from Braak, and (C) neuritic plaque score modified from CERAD.